SATELLITE REMOTE SENSING FOR MONITORING COASTLINE DYNAMICS OF THE CANADIAN BEAUFORT SEA COAST

Anton Vrieling
Joost van der Sanden

November 2000

Canada Centre for Remote Sensing

Geomatics Canada

SATELLITE REMOTE SENSING FOR MONITORING COASTLINE DYNAMICS OF THE CANADIAN BEAUFORT SEA COAST

Anton Vrieling
Wageningen University

Joost van der Sanden
Canada Centre for Remote Sensing

November 2000

Summary

Coastal zones are of great ecological and economical importance. Nevertheless, they are threatened by coastal erosion, which forms an increasing global problem. Reliable and timely information on coastal dynamics is a prerequisite for more sustainable management of coastal zones. Satellite remote sensing has the potential to provide this type of information. The present study aims to develop a procedure for extracting coastlines from a variety of satellite remote sensing data and to apply this procedure to map the dynamics of the Canadian Beaufort Sea coastline. This coastline has been reported to be particularly sensitive to erosion and hence to the impact of sea level rise.

The Canadian Beaufort Sea coastline forms part of an arctic region. It has a generally low relief of less than 60 m and is composed of unconsolidated sediments, which are bonded by ice. The warm water of the Mackenzie River exerts a great influence on the area, by inducing thaw settling of the sediments and fastening break-up of the sea ice. During the open water season (July-September) storm winds may generate high storm surges over ice-free fetches. Jointly, these processes destabilise the coast and induce rapid coastal retreat. The coastline of the active delta is retreating most rapidly. The process of global warming is expected to accelerate coastal erosion in the future.

Various methods for coastline extraction are described in literature. Most of these methods are designed especially for either optical or radar imagery. In this study, a variety of images were used, including a Landsat MSS image of 1973, a Landsat TM image of 1986, four SPOT panchromatic images of 1991 and a RADARSAT W2 image of 1999. Hence, it was necessary to select a method that could serve to extract coastlines from different image types. The approach adopted may be referred to as local region growing.

Image analysis started with the despeckling of the RADARSAT and then the scaling and geocoding of all images available. Next, coastlines were extracted by means of local region growing. Region growing is an iterative process in which regions are merged based on a homogeneity criterion. In this study the criterion used was a gray level threshold value. Local region growing applies the algorithm in various subregions. This allows setting different threshold values, and can therefore account for the variable land-water contrast in the image. The most subregions needed to be defined for SPOT panchromatic images, since they have the least contrast between land and sea. This results from the high reflectance of sediment-rich water in the visible spectrum.

Overall, local region growing provided a good estimate of the coastline position in the individual images. Positional inaccuracies are mainly due to flaws in the process of geocoding, the presence of mixed pixels, and incorrect threshold selection resulting from misinterpretations of the coastline position. To account for possible inaccuracies, trends in the temporal sequence of the four coastlines were used in the definition of erosional classes. Four classes were distinguished: rapid erosion (>5 m yr^{-1}), moderate erosion (1-5 m yr^{-1}), no detectable erosion (-1 - 1 m yr^{-1}), and accretion (<-1 m yr^{-1}). The resultant coastal erosion map shows rapid coastline retreat in the active delta in particular.

Uncertainties in the positional accuracy of the extracted coastlines are believed to be too high to make reliable assessments of temporal differences in erosion rates. Therefore, this study can neither confirm nor refute the expected acceleration in coastal retreat due to global warming. Yet, the dominant coastline dynamics of the Canadian Beaufort Sea could be mapped. This demonstrates the value of satellite remote sensing as a tool in support of coastal erosion studies.

In the future, the possibilities for the monitoring of coastal dynamics by means of satellite remote sensing are expected to improve, because (a) the time span for which data will be available increases, (b) the available image database is expanding as more satellites are being launched and (c) satellites with enhanced spatial resolution are being introduced. The success of any coastal erosion study depends heavily on the data available. In terms of wavebands, the application of either radar images or infrared images is recommended. In terms of spatial information content, the user will have to establish a compromise between spatial resolution and spatial coverage.

Table of contents

1. Introduction

Coastal zones are of great ecological and economical importance. Two-thirds of the world population live in these areas (Pirazolli, 1985) and they are an important habitat for birds and other wild life. However, coastal zones are physically unstable and vulnerable to natural and human impacts. A clear sign of this instability is erosion and the associated loss of land (Hanson, 1993).

Most of the world's shorelines suffer from coastal erosion (Pilkey, 1991). Coastal erosion is a natural process that causes the shoreline to retreat through forces executed by wind, water and ice. This process can be a big threat to human settlements and to fragile natural ecosystems. Global warming and the resulting sea level rise have a great impact on the rate of shoreline retreat. This is supported by studies that suggest an increased global erosion pattern (Bird, 1985). These developments indicate the need for strategies and tools that allow monitoring of shoreline morphodynamics. A monitoring system that can compare large parts of the shoreline would help to identify unstable coastal areas and give insight in the processes that determine the spatial variability of coastal erosion. Furthermore, such a system will help to plan mitigation strategies and assist in the development of models that can facilitate the prediction of future coastline dynamics.

Remote sensing can serve as a valuable tool for coastal erosion monitoring purposes. Satellite imagery is very suitable for change detection because of repetitive coverage of the same region. Furthermore, satellite images cover large areas, which makes them an excellent device to study large spatial patterns. As the spatial resolution of earth resource satellites is increasing even minor changes can be detected through satellite imagery. Because of this trend, the general availability of satellite imagery and its large ground coverage, satellite remote sensing provides a good tool for detecting shoreline changes (Chen and Rau, 1998).

Detecting changes is most straightforward using images of the same sensor at different dates. Starting from 1973 with the launch of Landsat-1, a variety of earth observation satellites have been acquiring imagery. Each sensor has its own characteristics like resolution (spatial and temporal), frequency and bandwidth. Imaging satellites operating in the microwave domain of the electromagnetic spectrum have an advantage over satellites operating in the optical domain, as clouds do not obstruct radar waves. However, it is only since 1991 with the launch of ERS-1 that radar satellite imagery became available on a continuous basis. It is a challenge to use images of different sensors for the monitoring of a natural phenomenon during time.

In this study, historical satellite images of various sensors are used to monitor shoreline dynamics. For this, a procedure is needed to extract the coastline from the imagery. A simple way to do this is through on-screen digitisation. However, this is a very labour intensive process. Several procedures have been proposed in literature for automatic coastline extraction from satellite imagery, most of them being specific for one sensor type (e.g. Blodget *et al.*, 1991; Lee and Jurkevich, 1990). Here, a procedure is needed that will allow to extract shorelines from a variety of images and compare them.

This study concentrates on the shoreline of the Canadian Beaufort Sea coast. This shoreline is amongst the ones most sensitive to sea level rise (Shaw *et al.*, 1994). Temperature is an important factor for coastal erosion in this arctic region. Shoreline retreat mainly occurs from June to early October, when open water is present that heavily increases the storm surges (Hill *et al.*, 1994). However, ice processes are also significant contributors to rapid coastal retreat (Héquette and Barnes, 1990). Over 80% of the coast is considered erosional with mean retreat rates greater than 1 m yr^{-1} (Harper, 1990), whereas rates up to 29 m yr^{-1} have been reported (Harper *et al.*, 1985). Global warming is thought to accelerate the erosion processes (Solomon *et al.*, 1993).

The objective of this study is to develop a procedure for extracting coastlines from a variety of satellite remote sensing data. Furthermore, this study aims at mapping the morphodynamics of the Canadian Beaufort Sea coastline from 1973 onwards. The results of this study will feed into the Canadian Coastal Information System of the Geological Survey of Canada (GSC) Atlantic. This will support modelling of coastal erosion and planning of mitigation strategies. In addition, the results of this study will contribute to phase 2 of the Mackenzie GEWEX (Global Energy and Water cycle EXperiment) Study.

The structure of the report is as follows. Chapter 2 gives a summary of the various analysis procedures for extracting coastlines from satellite remote sensing data, as described in literature. Chapter 3 portrays the Beaufort Sea Coast area, including the problem of coastal erosion. A description of the various remote sensing data and satellites used in this study can be found in chapter 4. Then, the applied procedure for coastline extraction is described in chapter 5. Subsequently, chapter 6 presents the results of the coastline extraction procedure and the derived data on coastline dynamics together with a discussion of these results. Finally, chapter 7 will draw the conclusions and recommendations for possible improvements will be made.

The authors would like to acknowledge Steve Solomon of the Geological Survey of Canada (Atlantic) for his collaboration and help. He let us tap into his extensive knowledge about the study area and provided valuable ground reference data, including the photographs as shown in chapter 3.

2. Remote sensing for coastal monitoring

Remote sensing methods have been used for the monitoring of coastal erosion for a long time. A large number of studies utilised aerial photography for the detection of historical changes in the shoreline (e.g. Dolan *et al.*, 1978; Stafford and Langfelder, 1971). Most studies examining coastal recession at the Canadian Beaufort Sea coast, also used aerial photography for the determination of erosion rates (e.g. Mackay, 1986; Solomon and Covill, 1995).

As frequent and repetitive data coverage is essential for effectively monitoring rapidly changing shorelines and the photogrammetric procedure of data acquisition is costly and time consuming, satellite imagery provides a good alternative for the monitoring of coastal changes. Moreover, satellite imagery provides a large ground coverage, which facilitates a regional comparison of coastal morphodynamics. Although the spatial resolution of aerial photography is usually higher, the resolution of satellite systems has increased considerably during the last two decades. This development results in high availability of historical images that will increase the precision in determining shoreline changes through satellite imagery.

Various methodologies have been used for shoreline monitoring using remote sensing. Some of them use techniques to jointly analyse images from different dates for the extraction of erosion/accretion patterns. Others focus on the extraction of coastline vectors from the imagery and subsequently compare these for different dates. Coastline detection in optical imagery differs significantly from detection in radar images (Lee and Jurkevich, 1990). The following review is therefore based upon this division.

2.1 Coastal monitoring using optical satellite remote sensing

A relatively simple method for investigating coastal erosion and accretion patterns is by using image processing techniques to jointly analyse images from different dates. Blodget *et al.* (1991) use six Landsat-MSS images and difference MSS band-7 (0.8-1.1 μm) of the images relative to the initial image. This results in an image composite showing the occurred change over the considered time periods as distinct colours. Frihy *et al.* (1994) and El-Raey *et al.* (1999) use a similar approach. Besides image differencing El-Raey *et al.* also calculate the ratio of images of different dates. This results in dark pixels for erosional areas and bright pixels for accretional regions. However, the derived morphodynamic patterns were similar to the ones obtained from image differencing.

Apart from combining images, monitoring can also be done through extracting the shoreline from a single image and subsequently compare shorelines of different dates. Unsupervised classification can serve to extract coastlines from multi-spectral images by dividing the images in land and water classes (Frihy *et al.*, 1998). Another way to extract coastlines that can also be applied to panchromatic images, is applying a threshold algorithm (Chen *et al.*, 1995). Using thermal infrared data from aerial imagery, Majumbar and Bhattacharya (1991) developed a method for automatic selection of this threshold.

A special approach to thresholding, which uses regional information, is called region growing. This method seeks to grow homogeneous regions by merging pixels on the basis of some similarity criterion (Le Moigne and Tilton, 1995). White and El Asmar (1999) apply a specified gray level difference from the region mean (a threshold) as the homogeneity criterion, to Landsat TM band 7. Region growing is initiated from the sea. Subsequently the region growth through canals and drainage channels is manually deleted, leaving only the coastline. This coastline is converted to vector format and compared for several image dates to derive coastal erosion and accretion patterns.

The capability of using neural networks as a tool for delineation of shorelines is demonstrated by Ryan *et al.* (1991). Neural networks are models composed of many simple processing elements

connected by links with variable weights. Ryan *et al.* first standardise the imagery, then accomplish a coarse categorisation of land and water. This categorisation is done by dividing the image in blocks, calculating texture measurements for each block, which are subsequently fed to a neural network classifier, described by Rumelhart and McClelland (1986). The land-water boundary is converted into a shoreline strip, in which a convolution filter and a threshold level identify boundary candidates that are connected through a connectivity algorithm.

In coastal regions with considerable tidal dynamics, differences in tidal elevations between images have to be accounted for. Chen and Rau (1998) create a reference digital terrain model (DTM) from a set of multi-spectral SPOT images, acquired in the same year at different tidal elevations. Shorelines are digitised manually and assigned the value of the tidal elevation at that time. These contour lines are interpolated to create the DTM. For the image to be compared with the DTM, shorelines are digitised as well. On the reference DTM the shoreline is traced for the specific tidal elevation of the image under consideration. Changes between the two reflect the shoreline dynamics between the date of the reference DTM and the image.

2.2 Coastal monitoring using radar satellite remote sensing

A possible approach to identify areas of morphological change is by superimposing a satellite image on an older topographic map. This approach has been followed by Singhroy (1996) and Barbosa *et al.* (1999) with RADARSAT-1 data. However, to analyse occurring changes between two image dates, a different methodology is needed. Because of the specific data acquisition technique of Synthetic Aperture Radar (SAR) systems, that produces artefacts like speckle, a simple combining of images by division or subtraction as reported for optical imagery, would be difficult to accomplish. Therefore, coastal studies using SAR imagery focus on shoreline extraction procedures.

Speckle effects and the strong signal return from a wind-roughened, wave-modulated sea cause a frequent lack of contrast in SAR images. Therefore it is difficult to detect the shoreline by conventional methods like thresholding or segmentation by edge magnitude (Lee and Jurkevich, 1990). Reported detection algorithms exploit the fact that radar backscatter from ocean areas is generally more homogeneous than from land areas. Furthermore, most methodologies use two levels of spatial resolution: first a coarse separation of land and water is made, which is followed by a fine tuning and tracing at full resolution.

Lee and Jurkevich (1990) describe a method for coastline detection from SAR images using a chain of basic image processing operations. They first reduce speckle by applying a sigma filter, followed by a Sobel edge operator (Pratt, 1978) to generate a preliminary edge map. Then a mean filter is applied to fill gaps between neighbouring pixels. As the sea is more homogeneous, it has a lower gray level in the edge map, so thresholding serves to separate sea from land. Subsequently a tracing algorithm is applied for delineation of the coastline. Because of the mean filter, the traced coastline is situated some pixels seaward of the coast. Therefore, a refinement is executed by applying a mean filter to the coastline, thresholding of the result and retracing the inside edges.

A different approach for coastline detection that aims at higher positional accuracy is proposed by Mason and Davenport (1996). They use a hierarchical processing approach in which the coarse resolution processing stage determines the approximate location of the coast, and a full resolution stage performs the contour tracing. At coarse resolution a contrast ratio edge detector (Touzi *et al.*, 1988) and a hysteresis thresholding algorithm (Canny, 1986) are used to detect sea regions as areas of low edge density. Image areas near the shoreline are subsequently subjected to more elaborate processing at high resolution using an active contour model (Kass *et al.*, 1987).

A method that is similar to the one proposed by Mason and Davenport (1996), is presented by Niedermeier *et al.* (2000) and also adopted by Romaneessen *et al.* (2000). Similarities are the hierarchical processing approach, the detection of sea regions as areas of low edge density and the use of an active contour model (also called snake algorithm). The main difference is the way edges are found. For that purpose, a continuous wavelet transform (Zhong, 1990) is calculated for the logarithm of a SAR image. Subsequently, an adapted version of Mallat's wavelet-based edge detection method is applied (Mallat and Hwang, 1992; Mallat and Zhong, 1992), which results in a separation of edges and noise by thresholding. In both studies, ERS images are used for the extraction of coastlines that are exploited for DEM interpolation, indicating bottom topography of the Elbe estuary in Germany.

The wavelet transform is also applied by Bijaoui and Cauneau (1994) to separate textural information from radiometry. They treat speckle as a surface type characteristic. If the sea surface is uniform, the speckle texture will be stationary as opposed to land areas. This texture is described by a co-occurrence matrix (Pratt, 1978), which is calculated for a training area, defined as the sea case. A decision rule is formulated to accept or reject pixels by setting a threshold for the distance between the co-occurrence matrix for a given pixel and the reference matrix. The distance between the two matrices is defined in Tou and Gonzalez (1979).

Zhang *et al.* (1994) transform a filtered SAR image into a feature space by calculating the absolute deviation from the mean value over a 7x7 moving window, which reflects the roughness of an image. Their sea-land separation is based on the idea that adjacent pixels are likely to be from the same region type as the majority of its neighbours. This spatial continuity assumption is reflected in the theory of Markov Random Fields (MRFs). An MRF is a discrete stochastic process whose global properties area controlled by means of local properties (Chellappa and Jain, 1993). Descombes *et al.* (1996) use MRFs at two levels of spatial resolution in a hierarchical approach. Basically, their methodology consists of executing multi-class segmentation, as they state that bimodal histograms are not always a valid assumption in SAR images. Then they impose spatial continuity between adjacent regions, using a holes topology. This topology consists of 8 connectivity neighbours and 8 neighbours located at a certain distance. If a given pixel does not have the same value as the corresponding 8 distant neighbours, it is reversed. Simulated annealing is applied to obtain the final result.

Apart from looking at one SAR image at the time, a technique called repeat pass SAR interferometry can also help in the detection of a coastline. SAR interferometry compares the phase difference of two radar images, separated by a certain time period. Coherence maps describe the degree of stability of the complex scatterers between the two acquisitions. Schwäbisch *et al.* (1997) use the coherence information of ERS tandem data for distinguishing between land and sea surfaces. Land surfaces are highly correlated compared to the decorrelated water surfaces. By detecting large coherence value gradients, the coastline can be delineated.

3. The Canadian Beaufort Sea coast

The study area comprises a large part of the Canadian Beaufort Sea coast, which includes the Mackenzie Delta. It is an arctic region between 68º and 70º northern latitude and between 132º and 137º western longitude. The location of the study area is shown in figure 3.1.

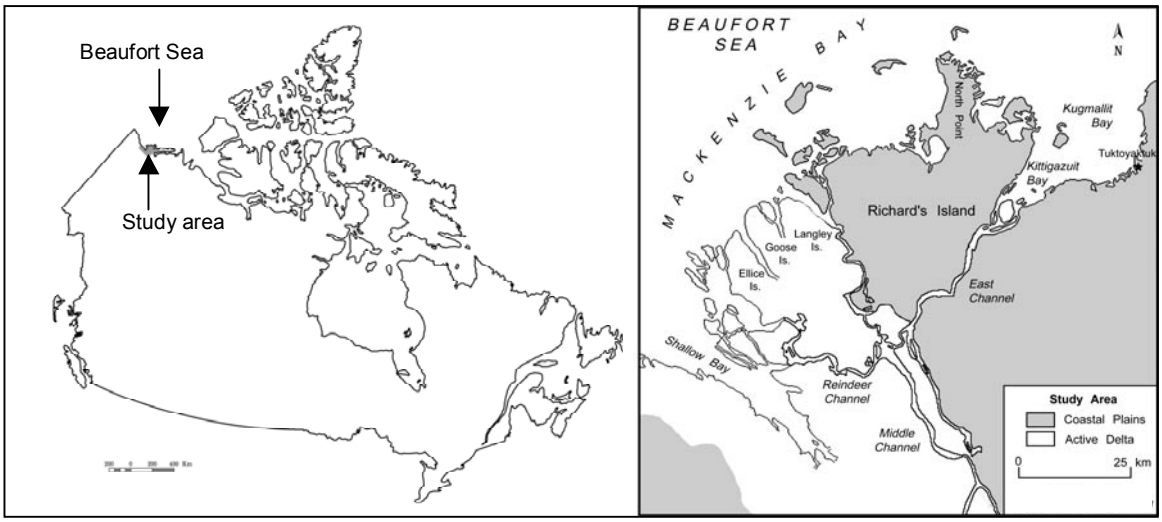

Figure 3.1 The location of the study area in Canada (left), and at the right a detail of the area (after De Abreu *et al.*, prep.).

3.1 Coastal geology and geomorphology

The Canadian Beaufort Sea coast has a generally low relief of less than 60 m throughout the region (Ruz *et al.*, 1992). The coastline is composed of unconsolidated sediments, including sand, gravel and glacial diamict, which are bonded by ice (Rampton, 1982, 1988). Ground ice contents are high in the area (Dallimore *et al.*, 1996). It occurs in discrete bodies of massive ice (Mackay, 1971), pingos (Mackay, 1962), ice wedges (Mackay, 1963), buried snow bank ice (Pollard and Dallimore, 1983), thin ice lenses and coatings, and ice in soil voids (Pollard and French, 1980).

A widespread characteristic beneath land areas is the presence of permafrost, which may reach up to 700 m of depth (Burgess *et al.*, 1982). At the ground surface, mean annual temperatures are between –8 and -9ºC (Kurfurst and Dallimore, 1991). Permafrost continues in continental shelf sediments offshore, but is presently degrading, because of the warming effect of the sea (Hunter, 1988). Where sea ice freezes to the bed in winter, at waterdepths less than 2 m, permafrost is preserved through negative mean annual temperatures (Dallimore *et al.*, 1996).

Figure 3.2 Lakes near Tuktoyaktuk and two pingos in top left.

Figure 3.3 Fringing spit of Tuktoyaktuk (only village in study area).

A striking characteristic of permafrost-affected coastal plains (see figure 3.1) is the occurrence of numerous lakes formed by freeze-thaw processes (figure 3.2). The coastlines of these plains consist of broad embayments, narrow headlands and fringing spits (Hill and Solomon, 1999; figure 3.3). Harper (1990) gives a clear overview of the present coastal types at the Canadian Beaufort Sea coast. He defines six types of which four are erosional (ice-rich cliffs, ice-poor cliffs, low-tundra cliffs and inundated tundra) that comprise 60% of the coast. By definition, the other 40% are accretional landforms (barrier islands and spits, and deltas). However, as deltas in the study area are rapidly retreating, 80% of the coast can be considered erosional. The cliffs vary in height from less than 2 m to greater than 30 m (Hill and Solomon, 1999).

The Mackenzie Delta is a dominant feature in the area (figure 3.5). Having a mean annual flow rate of about 10,000 m^3s^{-1} of relatively warm water, the Mackenzie River exerts a great influence on the oceanography and ice cover in the delta region, with implications for coastal stability (Solomon *et al.*, 1993). Annual sediment input is about $150*10^6$ t and consists mainly of silt and clay (Davies, 1975).

3.2 Sea ice and coastal oceanography

The Canadian Beaufort Sea is completely ice-covered from October to June. Hayes (1979) classifies the coast as wave-dominated during the ice-free season. During this open water season, that lasts three to four months, ice-free fetches of more than 100 km are common (Solomon *et al.*, 1993). Winds during this period originate from the east, southeast and northwest quadrants, but storm winds (>40 km h^{-1}) are most common from the northwest. These storm winds create positive storm surges of up to 2.4 m (Harper *et al.*, 1988). The wave regime is characterised by wave heights of 4 m and periods up to 10s (Pinchin *et al.*, 1985). The most important water level changes are related to these storm surges, as the range of astronomical spring tides is no more than 0.5 m (Solomon *et al.*, 1993).

3.3 Coastal recession

Reported coastal retreat rates are high along the shoreline of the Canadian Beaufort Sea. Coastal recession can be expressed as volumetric erosion (m^3 yr^{-1}) per meter of shoreline or as linear erosion (m yr^{-1}). In this study we use linear erosion rates. Harper (1990) estimates mean retreat rates greater than 1 m yr^{-1} along the Canadian Beaufort Sea coast. Mackay (1986) reports average rates of 8 m yr^{-1} for ice-rich cliffs and 1 m yr^{-1} for sandy coastal bluffs over a 50-year period. Solomon and Covill (1995) report rates up to 20 m yr^{-1} resulting from the impact of one September storm. The highest reported rates in the area are 29 m yr^{-1} in the Mackenzie Delta (Harper *et al.*, 1985). The delta is the area of most rapid retreat (Harper, 1990).

The coastal environment is experiencing a combination of thermal erosion, wave influence and sea ice induced processes. Coastal and nearshore sedimentary processes may be significantly influenced

Figure 3.4 Two pictures showing an example of cliff erosion resulting from mechanical block failure.

during the freeze-up and break-up of sea ice through the action of various mechanisms such as ice-scouring, ice-push or ice-rafting (Ruz *et al.*, 1992). Héquette and Barnes (1990) show that ice-scour erosion of the nearshore seabed may change the equilibrium profile and lead to coastal retreat. However, Solomon *et al.* (1993) stress the overriding importance of storm waves as the main factor determining the rate of coastal recession. Kobayashi *et al.* (1999) summarise the following factors affecting coastal retreat: the grain size of cliff and beach material, cliff height, ice content, thaw settling, cliff orientation, and the degree of exposure to the marine environment.

During storms, significant cliff erosion occurs as storm surge permits large waves to break directly on the cliff face. Cliff erosion occurs in several stages (Dallimore *et al.*, 1996): first a layer of thawed and slumped material is being removed through wave action, then waves undercut the newly exposed frozen cliff face, which results in a mechanical failure of the cliff due to gravity forces (figure 3.4). Because about 70% of the material above sea level is ice (Mackay, 1986), there is little replenishment of sediment in the nearshore area. As Kurfurst and Dallimore (1991) find that a main difference between a stable coastal site and an actively eroding site is the waterdepth in the nearshore area, this low replenishment of sediment implies that favourable conditions for coastal recession are being maintained.

Deltas are retreating even more rapidly than the cliffs, in spite of the sediment supply by the Mackenzie River. However, this sediment is easily mobilised and does not accumulate at the site (Solomon and Covill, 1995). Furthermore, the bluffs are very low (figure 3.5) and consist of fine-grained, ice- and organic-rich materials that can be removed easily when thawed. The retreat depends entirely on the ablation rate of the material, which is a function of temperature differences between water and the frozen material and the water velocity (Kobayashi and Atkan, 1986). Retreat is rapid under any conditions, although storms greatly affect the rates (Solomon and Covill, 1995).

Climate change has a huge potential effect on coastal erosion at the Beaufort Sea coast (Solomon *et al.* (1993). The Arctic Ocean (including the Beaufort Sea) experiences significant warming as a consequence of the greenhouse effect (Quadfasel *et al.*, 1991), although additional causes have been suggested (Grotefendt *et al.*, 1998). The present rate of sea level rise in the Canadian Beaufort Sea does not exceed a maximum of 2.5 mm yr^{-1} (Hill *et al.*, 1993). However, this warming also results in a substantial retreat of sea ice (Walsh, 1991), which has been observed for a period of 16 years using microwave remote sensing images (Johannessen *et al.*, 1995). This sea ice retreat will lead to longer open water seasons, which implies an increase in the probability of the occurrence of large fetches and severe storms that generate high storm surges and large waves. Furthermore, the increase in sea water temperature will increase the thermal and mechanical erosion of frozen sediment exposed to wave and current action (Kobayashi *et al.*, 1999). Therefore, it can be expected that the already high coastal retreat rates will augment even more in the future.

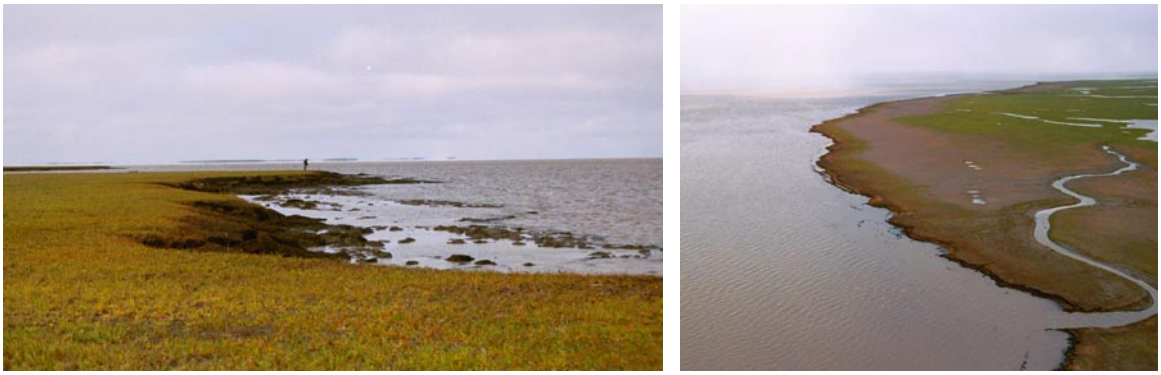

Figure 3.5 Two photos of a part of the active delta (Ellice Island), illustrating the low bluffs.

4. Remote sensing data

The present chapter discusses characteristics of the remote sensing data used in the study. This discussion is preceded by a short introduction to satellite remote sensing.

4.1 Satellite remote sensing

Since 1972, many satellites have been launched that are dedicated to measuring properties of the earth's surface. On July 23rd 1972, ERTS-1 (Earth Resources Technology Satellite) was the first to be brought into orbit. Later this satellite was renamed Landsat-1. At present, a great database of available images exists from a variety of satellites that have been or are in orbit. These include satellites that operate in the optical domain of the electromagnetic spectrum and those that operate in the microwave domain.

Optical remote sensing uses the optical spectrum, which extends approximately from 0.3 to 14 μm. This includes UV, visible, near-, mid-, and thermal infrared (IR) wavelengths. It is termed the optical spectrum because lenses and mirrors can be used to refract and reflect such energy (Lillesand and Kiefer, 1994). Optical systems operate in a passive manner as they sense naturally available energy. This energy can be separated into a number of wavelength ranges (bands), through prisms and gratings that act like filters. The final result is an image that contains several bands, which represent the energy sensed within the specific wavelength range for each resolution cell. This operation mode is called a multispectral scanner (MSS). However, also panchromatic images can be made with some satellites. In this case one (usually wider) wavelength range is used to create an image with higher spatial resolution. The spatial resolution is dependent on the system's *instantaneous field of view* (IFOV). The IFOV is expressed as the cone angle within which incident energy is focused on the detector. The optical systems most commonly used for earth resource monitoring applications are Landsat and SPOT (Satellite Pour l'Observation de la Terre).

Radar remote sensing uses the microwave portion of the electromagnetic spectrum, with wavelengths ranging from 1 mm to 1 m. Radar is an acronym for *radio detection and ranging*. Contrary to optical systems, radar is an active system, which implies that it supplies its own source of illumination. Advantages of radar are the capacity to image through clouds and by night. For imaging radars, pulses of microwave energy are transmitted to the scene, using an antenna that is pointed to the side (see figure 4.2), and subsequently the strength and origin of the echoes are recorded. The position can be determined from the time interval between transmission and reception of the signal. Radars measure the position in slant range along the line-of-sight of the radar to each reflecting object. This can be converted to ground range by correcting for incident angle. Incident angle is defined as the angle between the radar line-of-sight, and the local vertical with respect to the geoid. The energy is transmitted at a single wavelength, with a slight deviation that is called the bandwidth. The bandwidth is inversely proportional to the range resolution (perpendicular to the flight line). The pulse repetition frequency and the width of the antenna beam determine the azimuth resolution (along flight line). Synthetic aperture radar (SAR) systems allow the azimuth resolution to increase through using Doppler shifts of the received waves and processing techniques that synthesise the effect of a very long antenna. Although more SAR satellites have been and are in orbit, the most often used are ERS-1 and 2 (European Remote Sensing satellite) and RADARSAT-1.

4.2 Satellite images used in study

The images used in this study were acquired during summer (July-August) to minimise difficulties in coastline interpretation due to the presence of ice. They include Landsat MSS, Landsat TM, SPOT HRV and RADARSAT images, of which characteristics are discussed below. Table 4.1 gives an overview of the used images.

Table 4.1 Overview of used satellite images

year	date	satellite	sensor	used band	Wavelength	swath width	# images
1973	26 July	Landsat-1	MSS	MSS 7	0.8 – 1.1 μm	185 km	1
1986	23 July	Landsat-5	TM	TM 4	0.76 – 0.90 μm	185 km	1
1991	14 July, 30 July	SPOT-2	HRV	panchromatic	0.51 – 0.73 μm	60 km	4
1999	9 August	RADARSAT	SAR	C-band	5.6 cm	150 km (W2)	1

Landsat MSS

A Landsat MSS image of July 26th 1973 of the Landsat-1 mission was used. The multispectral sensor covered a 185 km swath width in four wavelength bands: two in the visible spectrum at 0.5 to 0.6 μm (green) and 0.6 to 0.7 μm (red), and two in the near IR at 0.7 to 0.8 μm and 0.8 to 1.1 μm. These bands were designated as bands 4, 5, 6 and 7 (another sensor onboard was designated bands 1 to 3). The image has a spatial resolution of 80 m and happens to be free of clouds. Band 7 has been used as it showed the best contrast between land and sea, compared to the shorter wavelength bands (see figure 4.1).

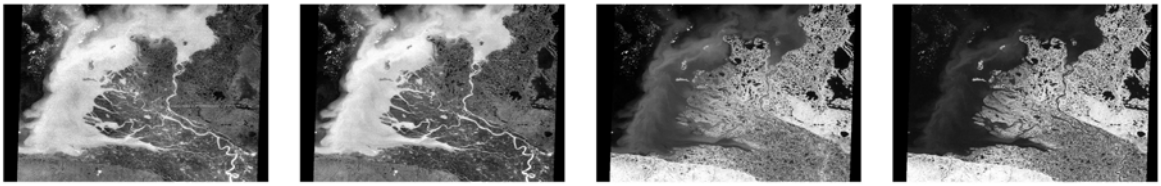

Figure 4.1 Original Landsat MSS image of July 26th 1973 with from left to right, bands 4 to 7.

Landsat TM

A Landsat Thematic Mapper (TM) image of July 23rd 1986 of the Landsat-5 mission was used. The TM is a multispectral sensor with a swath width of 185 km that measures in 7 bands. Table 4.2 lists the bands and their spatial resolution. The used image has cloud cover in some regions. TM band 4 was selected, being the most similar to MSS band 7 and showing a good land-water difference.

Table 4.2 Thematic Mapper spectral bands

band	spectral range	spatial resolution
1	0.45 – 0.52 μm (blue)	30 m
2	0.52 – 0.60 μm (green)	30 m
3	0.63 – 0.69 μm (red)	30 m
4	0.76 – 0.90 μm (near IR)	30 m
5	1.55 – 1.75 μm (mid IR)	30 m
6	10.4 – 12.5 μm (thermal IR)	120 m
7	2.08 – 2.35 μm (mid IR)	30 m

SPOT HRV

Three SPOT HRV panchromatic images of July 14th 1991 and one of July 30th 1991 of the SPOT-2 mission were used. SPOT-2 has two identical *high resolution visible* (HRV) systems, that can both operate in a panchromatic mode with 10 m spatial resolution and a multispectral mode (3 bands) with 20 m resolution. The sensor has a swath width of 60 km. The panchromatic mode uses the spectral range 0.51 to 0.73 μm and was used in this study. No cloud cover is present near the coastline in all four images.

RADARSAT SAR

RADARSAT-1 has one imaging instrument that is a SAR. It has five imaging modes that include Standard, Wide Swath, Fine Resolution, Extended and ScanSAR (see figure 4.2). In this study a Wide Swath 2 (W2) Path Image was used of August 9th 1999. W2 has incident angles between 31° and 39°, which is equivalent to 150 km swath width, and has a nominal spatial resolution of 30 m (changes with incident angle). Path Image refers to the processing level. A Path Image has been converted to ground range and satellite positional information has been added (georeferenced). Furthermore, multi-look processing has taken place. Multi-look processing reduces image speckle variance by the averaging of neighbouring pixels. In this case, 4 pixels in the azimuth direction were averaged. The next chapter gives more detail on speckle. The pixel spacing of W2 Path image is 12.5x12.5 m. RADARSAT operates at the C-band that has a wavelength of 5.6 cm. It has a HH-polarisation, which means that electromagnetic waves are horizontally transmitted and received.

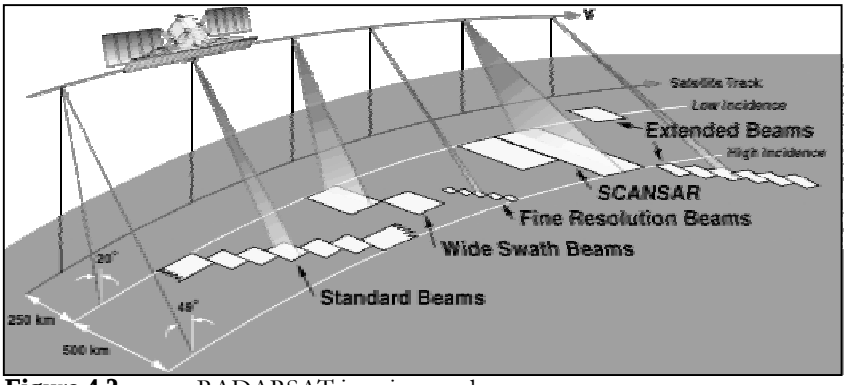

Figure 4.2 RADARSAT imaging modes

5. Methodology

There are various approaches to extract coastline dynamics information from satellite images (see chapter 2). When working with data from different sensors, the best option is to extract coastlines from each image and subsequently analyse them. For example, approaches like image differencing would not be possible to execute. Many methods for coastline extraction are specific to one sensor type and require a lot of processing steps. Furthermore, these methods do not guarantee a good result in problem areas (e.g. windy conditions, presence of sediment in water). Therefore, in this study a relatively simple semi-automated approach was adopted, that is called local region growing. The same approach could be used for analysis of all images. However, before doing so, several pre-processing steps were taken, which include despeckling of the RADARSAT image, scaling of the images, and geocoding. The different pre-processing steps are described in detail below.

5.1 Despeckling

A SAR is a coherent imaging system, which means that the phase structure of the transmitted signal is systematically retained through time. A characteristic of such a system is that it produces speckle. Speckle is the statistical fluctuation or uncertainty associated with the brightness of each pixel in the image of a scene (Henderson and Lewis, 1998). The effect arises because a resolution cell mostly contains a number of discrete scatterers. Each scatterer causes a phase and amplitude change to the backscattered wave. As the brightness within a resolution cell is the summation of the various backscattered waves, constructive and destructive interference will occur (see figure 5.1).

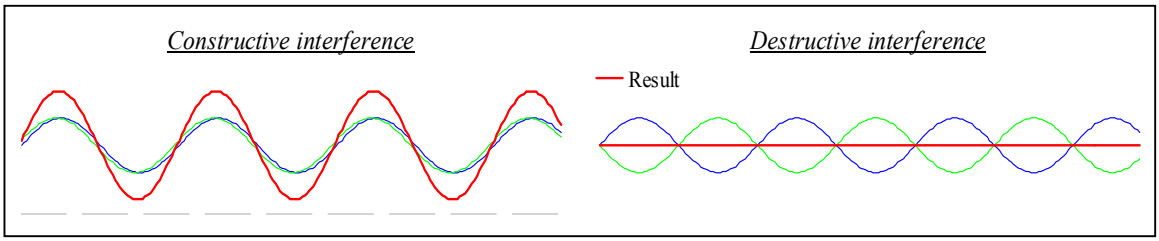

Figure 5.1 Constructive and destructive interference resulting in speckle.

Speckle gives an image a grainy appearance. Although speckle is often seen as unwanted noise, it can contain useful information. In this study it is preferred to reduce the image speckle variance, as the used coastline extraction method (described later) is hindered by its presence. The averaging of neighbouring pixels can reduce image speckle. A disadvantage of this method is that edges are not preserved, which is desirable for coastline extraction. Therefore, another speckle filtering approach is needed for subsequent processing.

A speckle filter is always a compromise between speckle removal and thin details preservation. Many filters exist that often show a similar performance. Considering the comparison made by Shi and Fung (1994), and taking as criteria a good speckle reduction plus the preservation of edges, the gamma MAP (maximum *a posteriori*) filter (Lopes *et al.*, 1993) was chosen. This filter aims at removing speckle while preserving edges, lines and point features. It determines the coefficient of variation C_A within a small square window around each pixel, which indicates the presence of heterogeneity in the local neighbourhood. C_A is calculated using the observed intensities I, that are expressed in terms of sigma nought (σ^0). Sigma nought represents the average reflectivity of a horizontal material sample, normalised with respect to unit area on the horizontal ground plane. C_A can be calculated through the division of the standard deviation of I by the average intensity value I in the filter window. Subsequently, C_A is evaluated against two thresholds and the estimation of the true radar reflectivity R_e is made as follows:

$$
\begin{aligned}
&R_e = \bar{I}, && \text{if} \quad C_A \le C_u \\
&R_e = ((a - N_{eq} - 1) * I + \sqrt{d}) / 2a && \text{if} \quad C_u < C_A \le C_{max} \\
&R_e = I && \text{if} \quad C_A \ge C_{max}
\end{aligned}
\tag{5.1}
$$

where: N_{eq} = equivalent number of looks

$C_u = 1 / \sqrt{N_{eq}}$

$C_{max} = C_u * \sqrt{2}$

$a = (1 + C_u^2) / (C_A^2 - C_u^2)$

$d = 4 * (a - N_{eq} - 1)^2 * N_{eq} * a * I * \bar{I}^3$

In addition, isolated pixels of very high or low gray value in homogeneous areas are removed following Lopes *et al.* (1990).

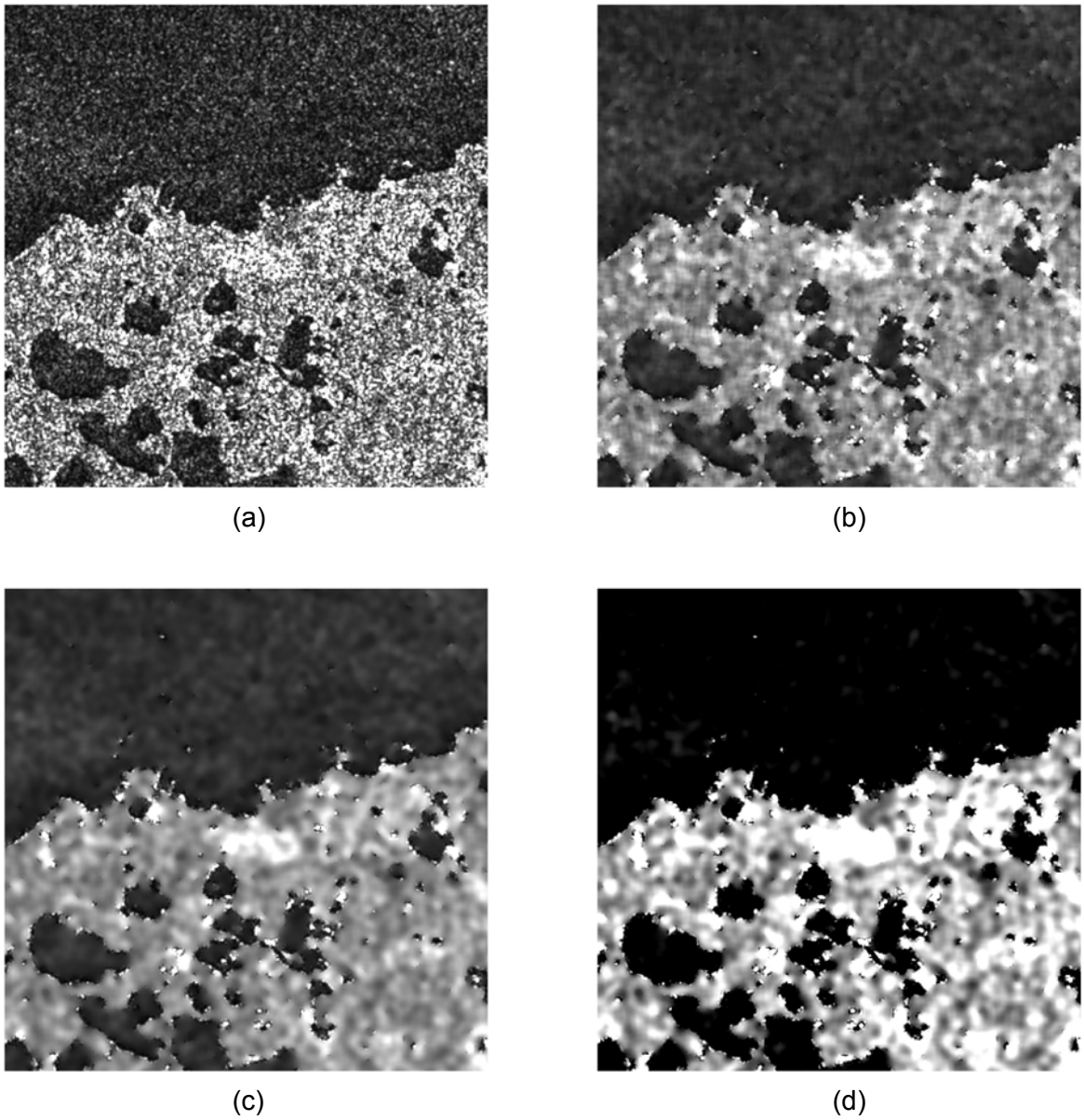

Figure 5.2 Iterated despeckling using 7x7 gamma MAP filter, shown on a subset of original RADARSAT W2 image (a), after 1 iteration (b), 2 iterations (c), and after 2 iterations with the scaling used for the complete image (d).

From equation 5.1, the equivalent number of looks (N_{eq}) deserves more attention, as it is a system's characteristic that needs to be calculated prior to speckle filtering. N_{eq} is defined to be the ratio of the mean squared to the variance for a homogeneous region of an image (Raney, 1998). It determines the number of degrees of freedom in the data.

To increase speckle reduction, the gamma MAP filter can be applied several times to the image as suggested by Oliver and Quegan (1998). Although they achieve good results with 8 iterations, in this study only two iterations were applied to the RADARSAT image. Selecting several homogeneous areas in the image, N_{eq} was calculated before both iterations and the results were respectively 3.3 and 17. A 7x7 window was used for the speckle filtering. Results for a small subset of the image are shown in figure 5.2 a, b and c. The second iteration proved to effectively create a greater reduction of speckle, with preservation of edges.

5.2 Scaling

Scaling is used to stretch the range of gray values in an image for visual enhancement. This facilitates visually distinguishing land from water. For all images, a certain gray level was set as minimum and another level as maximum. Subsequently the images were linearly stretched between those values towards a range from 0 to 255 (8-bit format). In the case of the SPOT images, it was tried to get a similar result for both image dates. The effect of scaling on part of the RADARSAT image can be seen in figure 5.2 d.

5.3 Geocoding

The speckle filtering has to be done before geocoding. However, geocoding does not necessarily have to precede coastline extraction. Valid reasons exist to do the geocoding after coastlines have been extracted and convert the coastlines along with the imagery. The most determinative would be the avoidance of resampling, which introduces an error to the coastline location. On these grounds, Shoshany and Degani (1992) recommend this working order. Nevertheless, other studies first perform geocoding (Chen and Rau, 1998; White and El Asmar, 1999). The main reason why it was chosen to do the geocoding first, is to ascertain if a good fit between the images can be obtained. Especially in change detection studies, a precise fit is essential. Furthermore, this allows preliminary assessment whether coastline changes are occurring and can be detected, before starting the rest of the process. Without geocoding it is not possible to overlay two images, which makes it hard, if not impossible, to visually pre-assess the occurrence of coastline change.

During geocoding, an image is transformed to a defined coordinate system. The coordinate system chosen in this study was the Universal Transverse Mercator (UTM) with the North American Datum of 1983 (NAD83). This transformation can be a polynomial function that mathematically describes how the uncorrected image has to be warped to match the coordinate system. It merely determines where the output pixel lies on the input image. Resampling of the gray levels of input pixels is required to calculate the gray level for the output pixel. In the present study, nearest neighbour resampling was chosen to preserve clear gray level shifts at the coastline. This method simply takes the gray value of the input pixel nearest to the transformed point as the value for the resampled output pixel. The output pixel size chosen was 10x10 m, so the highest resolution images (SPOT panchromatic) would not lose any detail.

For a precise transformation of an image, ground control points (GCP's) need to be collected for the calculation of the polynomial function. A GCP relates a location of a point in an image to the coordinates of that point in the chosen system. The most accurate result is obtained when many points are collected that are well distributed over the entire image.

The first set that has been geocoded, were the SPOT panchromatic images. Because their resolution is the highest, they have the best precision for determining the location of a certain feature. As hardly any manmade structures are present in the area, the land-water boundaries of the lakes were used for identification of GCP's. The lakes tend to have very steep, stable shores. This makes that possible water level changes do not significantly affect their circumference and location (pers. com. S. Solomon, GSC Altantic). In contrast, the coastline is very dynamic and hence not suitable for GCP collection.

A part of the GCP's was taken with the help of the online ground control database of the CCRS (http://geogratis.cgdi.gc.ca/) that has 3 m accuracy. Unfortunately, this database does not cover the complete region. Therefore 1:250,000 topographic maps (Energy, Mines and Resources Canada, 1988; 1989a, 1989b; Natural Resources Canada, 1996) had to be used, as accurate larger scale maps (e.g. 1:50,000) were not available. Larger scale maps or ground control points collected in the field by a Global Positioning System (GPS) could significantly improve the accuracy of the geocoding results.

In the SPOT case, the three images of July 14th 1991 were joined, which could be easily done, because they are from the same satellite orbit. Then, GCP's were collected and a first order polynomial transformation was executed. For the fourth image of July 30th 1991, a part of the GCP's was gathered from the intermediate geocoded SPOT image to allow a smooth transition between the images, and the other part from the above mentioned sources. Again, a first order polynomial transformation was executed for the fourth image, thus creating the final geocoded SPOT mosaic.

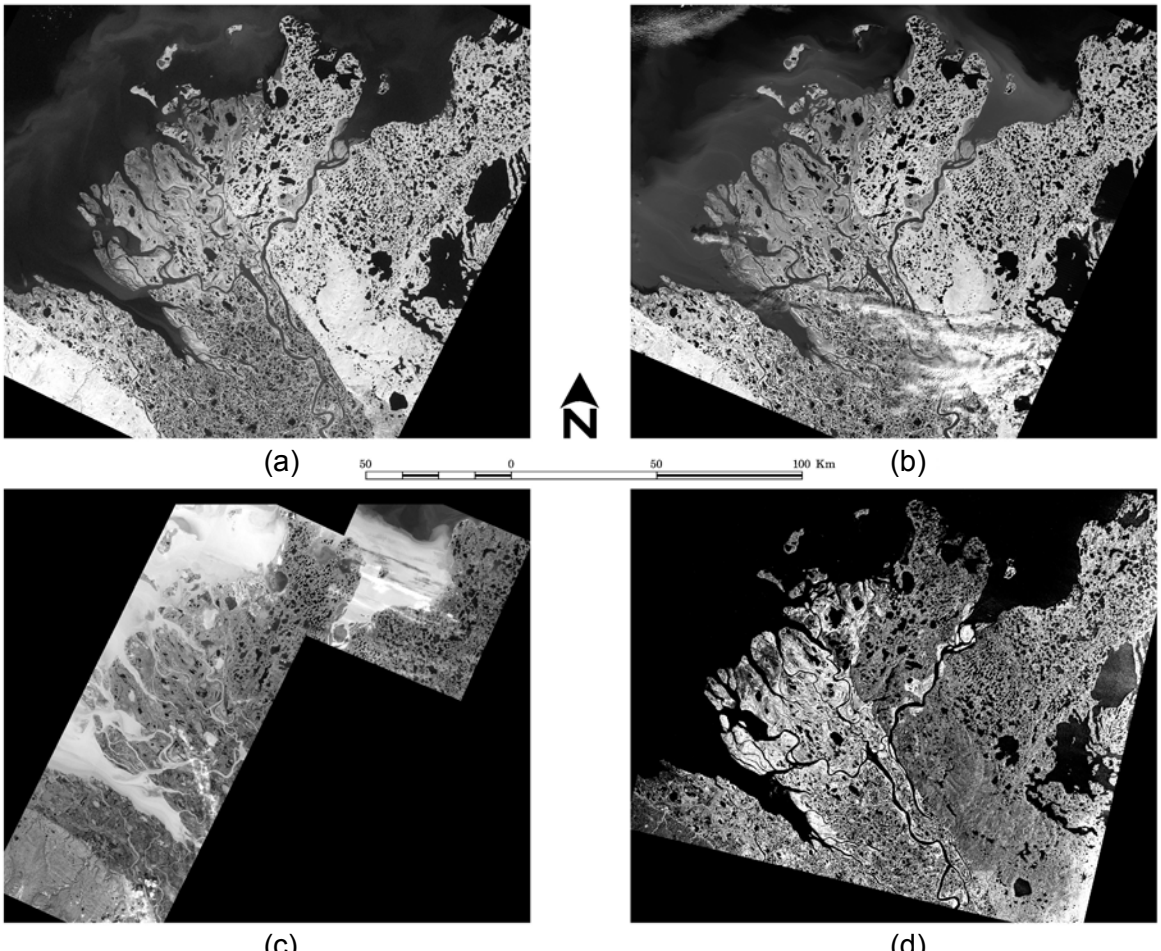

Figure 5.3 Overview of geocoded images: 1973 Landsat MSS band 7 (a); 1986 Landsat TM band 4 (b); 1991 SPOT panchromatic mosaic (c); and despeckled 1999 RADARSAT W2 (d).

This mosaic was then used as a base for geocoding the other images (Landsat MSS, TM, and RADARSAT). GCP's were collected again for the three images and fourth order polynomials were used for the transformation. The resulting geocoded images can be seen in figure 5.3.

Several sources of error may exist in the process of geocoding. The most important issue in this study is the fit between the images. This depends mainly on the distribution of GCP's over the image, the quality of GCP's, the transform model and the resampling method. Between 45 and 63 GCP's have been collected for each image, having a good distribution over the covered area. The absence of distinct features in the area of interest (e.g. manmade structures) complicated the collection of GCP's. However, visual uncertainties in the point placement are believed to average out when a large number of GCP's are identified. The transform model for the SPOT images is selected to be first order polynomial, hence no unwanted distortions occur in the mosaic. For the other images, a fourth order polynomial was chosen to optimise the fit. This fit can be analysed through the root mean squared (RMS) error. For the Landsat MSS image a RMS error of 0.36 times the resolution (80 m) was attained, whereas for the other images the RMS error was around half the resolution. Nearest neighbour resampling also introduces a certain error, because it tends to shift the image with a fraction of a pixel on average. However, every image was sampled to 10x10 m pixels and therefore this effect is negligible. Visual examination of the final results showed a good fit between all images.

5.4 Coastline extraction

As after geocoding, visual inspection revealed coastline change at several locations, the coastline extraction could be started. The extraction of the coastline from a satellite image is a segmentation problem in which the classes land and water need to be discerned. Image segmentation is the process by which individual image pixels are grouped into partitions, according to some intrinsic properties of the image (Le Moigne and Tilton, 1995). Although many segmentation techniques exist, no single method can be considered good for all images, nor are all methods equally good for a particular type of image (Pal and Pal, 1993). In chapter 2, a variety of coastline extraction techniques reported in literature were discussed. In this study, the segmentation technique of region growing has been

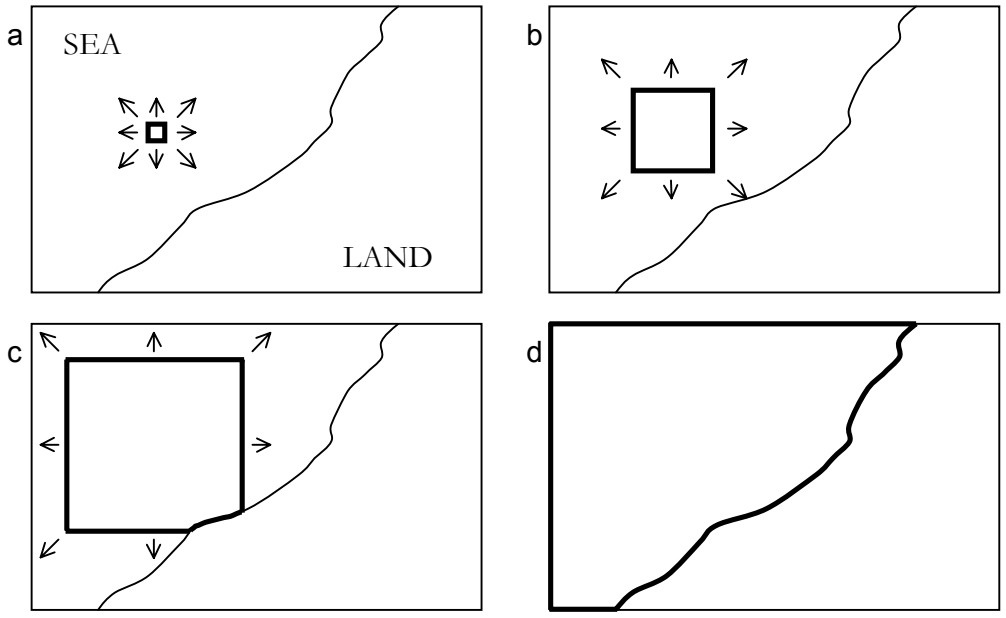

Figure 5.4 Diagram showing region growing segmentation. (a) A seed pixel is selected, and surrounding pixels are merged if they satisfy a homogeneity criterion. (b) the region continues to grow until (c) it encounters pixels that do not satisfy the criterion. (d) The algorithm finishes when the region can grow no further. (White and El Asmar, 1999)

applied. This technique was also used by White and El Asmar (1999), described on page 3 of this report. Figure 5.4 illustrates the technique.

Region growing is a region-based segmentation technique. Compared to edge-based segmentation techniques, it has the advantage of providing closed regions. In this study it is applied using gray level thresholds, but it can also be based on other homogeneity criteria, like for example texture (Lira and Frulla, 1998). Reasons for the choice of this method are the formation of a continuous coastline, the applicability to all images and its simplicity, which makes effective user interaction possible.

User interaction proved necessary, because of the complexity of the images, due to e.g. variable sediment loads of the water (mainly SPOT panchromatic), and local wind effects in the RADARSAT image. This makes that different thresholds need to be chosen within an image for an accurate segmentation of land and sea. Adaptive thresholding adjusts the threshold level to local criteria. In principle, it would be possible to introduce an automated adaptive threshold in the region growing process (Zucker, 1976). In this case, threshold selection would be based on some measure of the level of contrast found in a local window (e.g. Ching, 1994; Lie, 1995). Nevertheless, this would not allow distinguishing for example sediment-rich water and land surfaces in a SPOT panchromatic image as the same contrast level may be found. Therefore, the images were partitioned into subregions, for which different thresholds were selected manually.

Region growing was initiated from the sea and applied with the appropriate threshold in each subregion. Although guided by the land-sea contrast, thresholds were chosen through trial and error, accepting the value that resulted in the best description of the coastline. In accordance with the term 'local thresholding' (Taxt *et al.*, 1989), this process can be referred to as local region growing. In this case, it should be seen as a semi-automated method that substantially reduces required time in comparison with manual delineation, whereas a relatively high positional accuracy is maintained, that can be visually monitored during the process. The SPOT panchromatic mosaic needed most user interaction, since the wavelength band is particularly sensitive to suspended sediments and hence shows little land-sea contrast. An idea of the different images can be obtained from figure 5.3.

The geocoded Landsat MSS image of July 26th 1973 (band 7) was first processed. By creating a buffer of 500 m on both sides around the derived coastline, the area that needed to be considered in the other images could be reduced. Because Landsat MSS has the lowest resolution of the used images, it is most effective in cutting off small drainage channels during region growing, therefore restricting the land-water boundary to the real coastline. Local region growing was applied to the image, followed by a manual removal of inland lakes that were selected with the sea through small drainage channels. Subsequently a sieve filter was applied to eliminate small isolated pixel groups up to 2 MSS pixels in size. These small areas were removed because they are not believed to be actual islands. This results in a bitmap with classes land and sea. The same approach was applied to the other images within the buffer.

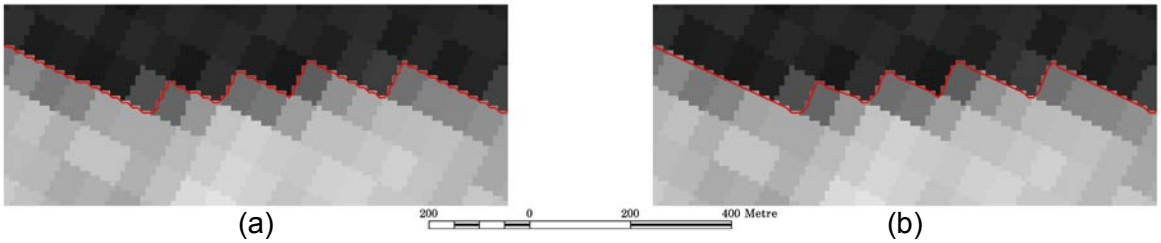

Figure 5.5 Influence of generalisation on extracted coastline of Landsat MSS, using bendsimplify with tolerance of 80 m; before generalisation (a) and after (b).

From the bitmaps, contour lines are created, which are subsequently smoothened through generalisation to remove small bends that result from the resampling of the image to 10x10 m pixels (see figure 5.5). This has been done using the bendsimplify option in the generalisation algorithm within Arc/INFO, specifying a tolerance equal to the resolution, which determines the degree of simplification. The outcomes of these operations are the final coastlines.

The described analysis results in four coastlines for 1973, 1986, 1991 and 1999. These can be used to derive data on coastline dynamics. The four coastlines were visually analysed and erosion classes were identified based on the change of coastline positions and the trend of this change. The result is a coastal change map of the Beaufort Sea coast. Figure 5.6 summarises the important processing steps described in this chapter to arrive at the coastline change map. The next chapter will provide a more detailed description of the map construction.

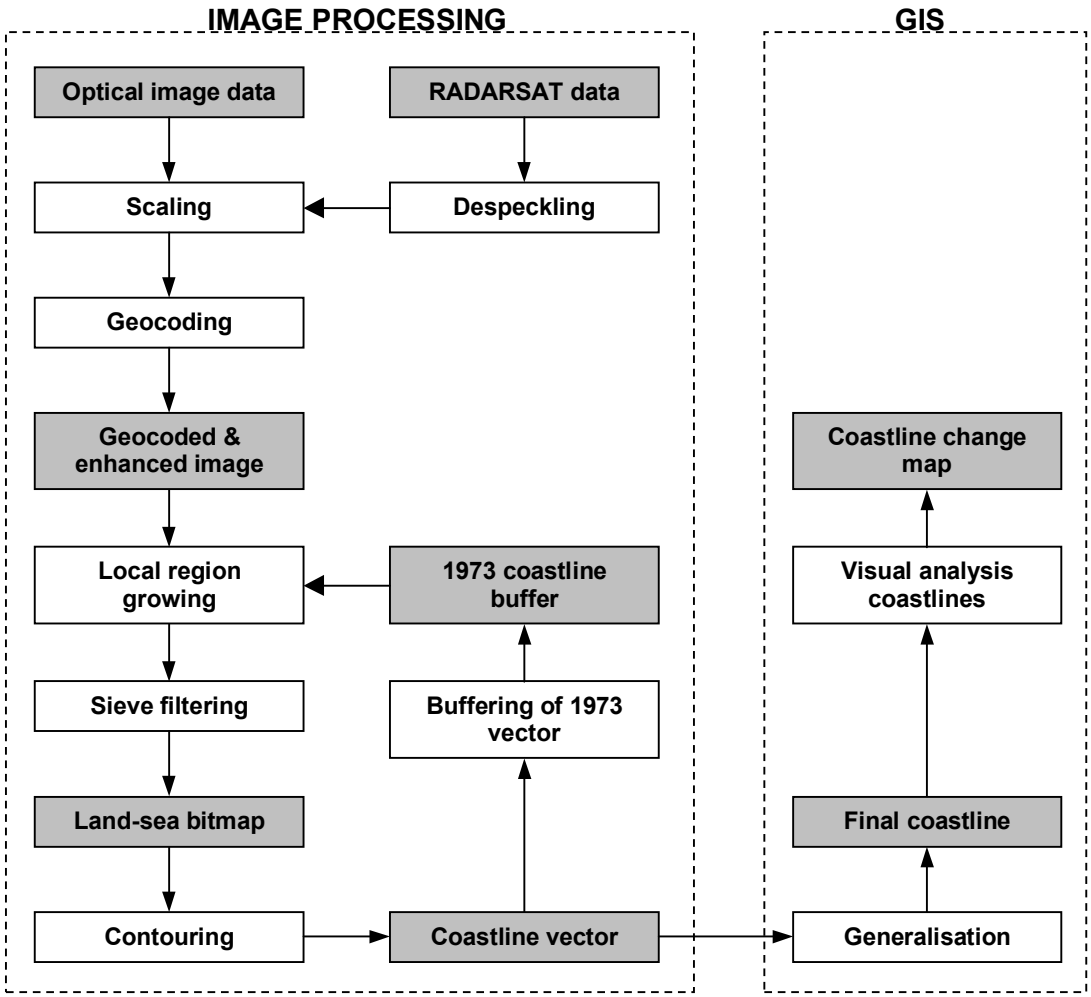

Figure 5.6 Schematic diagram showing the processing steps described in this chapter. Gray boxes indicate data products and white boxes indicate processing steps.

6. Results and discussion

In the previous chapter the methods have been described for the extraction of coastlines from the satellite imagery. This chapter will present the results of the applied methodology and use these for further analysis. The main outcome of this analysis is a map of the Canadian Beaufort Sea coast showing erosion classes along the coastline. The results will be discussed and possible improvements are suggested.

6.1 Coastline extraction

Applying the semi-automated procedure of local region growing, coastlines could be derived for all four images. The results can be seen in figure 6.1 for a small subset of the imagery. Especially in figure 6.1a, and to a lesser extent in figure 6.1b, the effect of resampling to a smaller pixel size is well perceptible in the image. Region growing will follow the blocky structure. Despite this, straight-line segments are being formed due to the generalisation algorithm (see also figure 5.5).

The figure also gives notion the influence of spatial resolution on the positional accuracy of the coastline. This can be explained by the presence of mixed pixels, i.e. pixels that comprise both land and water. This type of pixels is present in images of any resolution. However, they have greater implications for low-resolution images. Consider a Landsat MSS pixel that is oriented parallel to the coastline and composed of 50% land and 50% water. Depending on the threshold chosen, region growing may either select or not select the pixel. Given a pixel spacing of 80 m this implies a positional error of 40 m. In the case of SPOT panchromatic, this is only 5 m.

However, SPOT panchromatic has different problems that relate to the use of the visible spectrum. Reflection in this part of the spectrum is influenced by sediment in the water, which results in a general lack of contrast between land and sea. Therefore, many subregions needed to be defined during local region growing, which made the coastline extraction for this image a time-consuming task. To a lesser extent, sediment load also affects reflection in the near IR bands used for both the Landsat MSS and TM images (see figure 5.3a, b). To minimise sediment influences in the image, larger wavelengths should be used, like for example TM band 7 (2.08 – 2.35 μm). However, to be consistent with the selected MSS band 7, TM band 4 was chosen.

At times, it can be very difficult to perceive whether some features are part of the land or the sea. This complicates the threshold selection considerably. An example of this is illustrated in figure 6.1c. The pink arrows indicate an area that has probably been misinterpreted. Further to the right from the red interpreted coastline, another line can be observed. Comparison with the other images gives reasons to believe that this second line is more likely to be the true coastline. Interpretation errors by setting an inappropriate threshold are likely to exist in other images as well, although the SPOT image clearly has the least contrast. A problem that emerges in the Landsat TM image, is the presence of cloud cover over some coastal areas (see figure 5.3b). In the favourable case, these clouds are translucent, and local region growing can still be executed by defining a different subregion for the cloud-covered area. In a very small area, clouds were opaque and the coastline position has to be estimated.

Clouds do not obstruct radar waves and therefore the RADARSAT W2 image is free of cloud problems. Furthermore, a good contrast is present between land and sea in figure 6.1d. Apparently, the speckle filtering and subsequent scaling was a successful procedure. Radar backscatter is not directly affected by the sediment load of the water. Problems arise mainly when wind roughens the sea, which results in strong water return signals and hence a decrease in the land-sea contrast. This process is visible in the Kittigazuit Bay (figure 5.3d or 6.3, for location see figure 3.1).

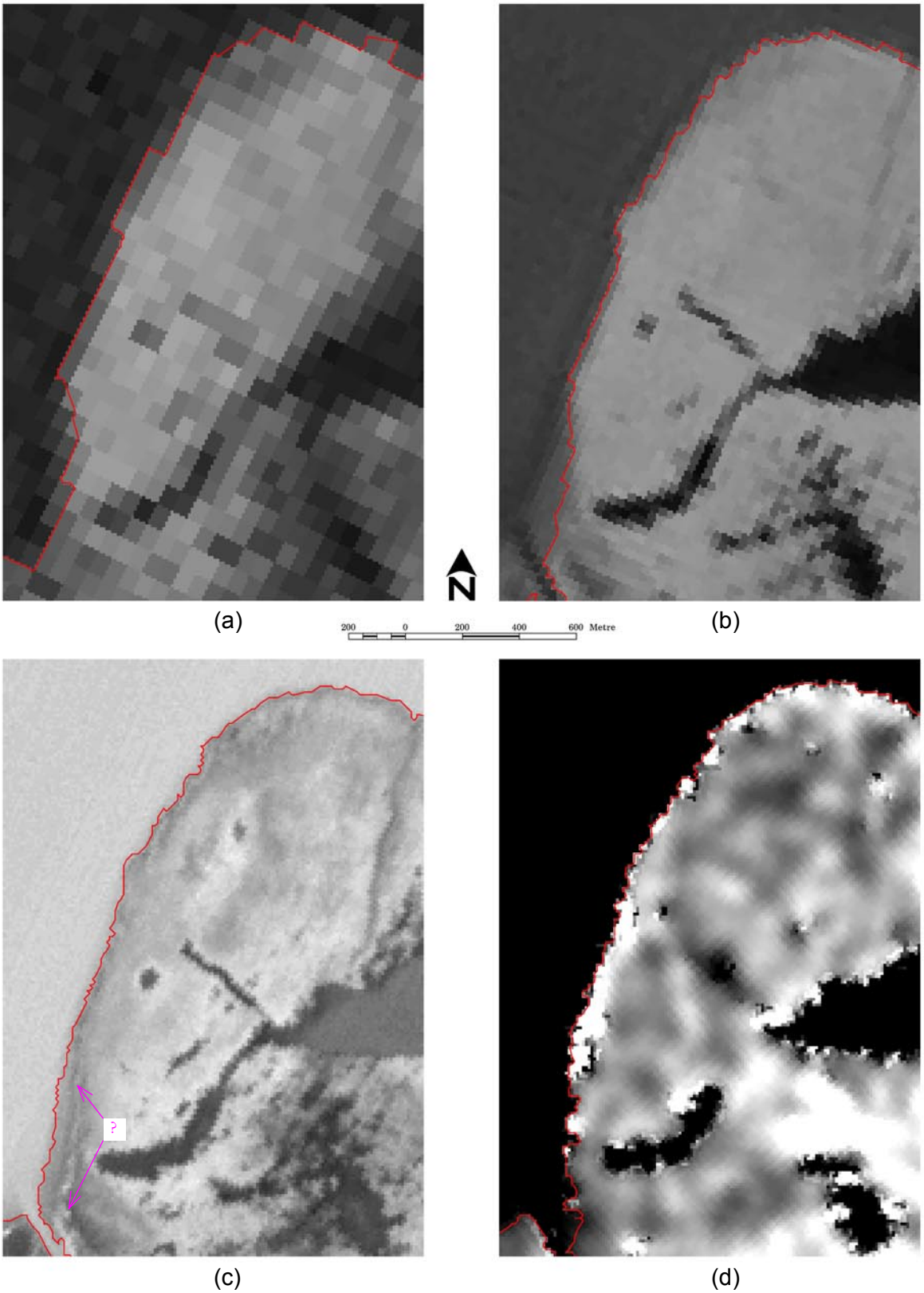

Figure 6.1 Fit of coastlines on subset of 1973 Landsat MSS (a), 1986 Landsat TM (b), 1991 SPOT panchromatic (c) and despeckled 1999 RADARSAT W2 (d) at location 1 in figure 6.3. The pink question mark in (c) indicates an area of confusion.

Given the limitations of the data, local region growing produced good results. It is a subjective approach in which the analyst visually determines the optimal threshold for each subregion. Contrary to fully automated methods, the analyst keeps a certain level of control. This is an advantage in complex images that are influenced by variable sediment loads (optical spectrum) or wind effects (radar) in an area that is characterised by highly irregular coastlines that are at places poorly defined. A disadvantage is that it requires more time on behalf of the analyst. However, most of the fully automated methods presented in chapter 2 are not applicable to both optical and radar images. Moreover, it is believed that these methods would not produce results as accurate as those obtained with the local region growing approach. This can be explained from the fact that the underlying assumptions of these methods are frequently violated in the large complex images (e.g. contrast may be the same for land and sediment-rich water). The extracted coastlines were used for the analysis of coastline dynamics, as presented in the next section.

6.2 Coastline dynamics

By comparing the derived coastlines, an analysis of its dynamics can be made. While analysing, error sources have to be kept in mind. A distinction should be made between errors resulting in a small offset of the coastline, which are caused by geocoding and the presence of mixed pixels (type 1); and errors resulting in offsets due to misinterpretations (type 2). Type 1 errors are estimated to not exceed the size of a resolution cell. This conservative estimate is based on a RMS error and mixed pixel error, both of which are in the order of half a resolution cell. The impact of type 2 errors is hard to quantify but may be substantially larger than 1 pixel (see figure 6.1c).

The availability of a temporal sequence of coastlines is an advantage in dealing with both error types. The relative position of the four coastlines assists in assessing the accuracy of the individual positions. Figure 6.2 shows the four lines for a rapidly eroding area. The lines are well separated, except for some minor line crossings, and the line sequence shows a clear trend of erosion.

Especially the trends help in defining whether a certain portion of the coast is subject to erosion or accretion or if it is stable, as they reduce the probability of errors of both types. The presence of a trend was used as a criterion in the coastal change map (figure 6.3) for classifying parts of the coast as erosional or accretional. The criteria for the different classes shown on the map are listed in table 6.1. The classes were defined in a conservative manner to account for the inaccuracies in the data and the methodology.

Table 6.1 Criteria for coastline dynamics map

class	erosion rate	sequence of coastlines
Rapid erosion	> 5 m yr^{-1}	Trend indicating erosion during total time span
Moderate erosion	1 – 5 m yr^{-1}	Trend indicating erosion during total time span
No detectable erosion	-1 – 1 m yr^{-1}	Same position coastlines, or absence of trend
Accretion	< -1 m yr^{-1}	Trend indicating accretion during total time span

The four coastlines were visually analysed for each portion of the coast, and a class was assigned for every location. Figure 6.3 shows large parts with no detectable erosion or accretion. In reality erosion or accretion may occur at these locations but either the rate of change was too slow to be imaged or a consistent trend was absent due to natural causes or error associated with the data sources and analysis method applied. The error contained in the map could be mitigated through the selection of different data. Higher resolution data reduce type 1 errors. Using data of the same sensor at the different dates could diminish type 2 errors. In this way, it is assured that the same features are observed in a similar manner. Accordingly, application of high-resolution data would be the key to reveal coastline dynamics that presently remain unobserved. It should be noted however that high-resolution satellite data from one and the same sensor have not become available until more recent years.

To assess the agreement between the erosion map and the ground truth, it would be good to compare the map with ground data or studies using aerial photography, which can reflect higher detail than the satellite data used. However, at the time of study, sufficient ground reference data were lacking to validate the coastline change patterns found.

In spite of positional inaccuracies, many parts reveal a clear erosional trend, like in figure 6.2. Figure 6.3 shows that the main erosion areas are found in the active delta of the Mackenzie River and the south shore of Shallow Bay in particular (figure 3.1). This agrees with Harper (1990) who describes the delta as the area of most rapid retreat. Several factors could explain the high erosion rates in this region. A great part of the water of the Mackenzie River flows into the active delta. This water is relatively warm and therefore accelerates thaw settling on the bluffs. As the bluffs are very low in the delta, and the coastal material is known to be erosion prone, the early thaw settling facilitates rapid coastal erosion (Kobayashi and Atkan, 1986). This is true for large parts of the active delta and the process is well described in chapter 3.

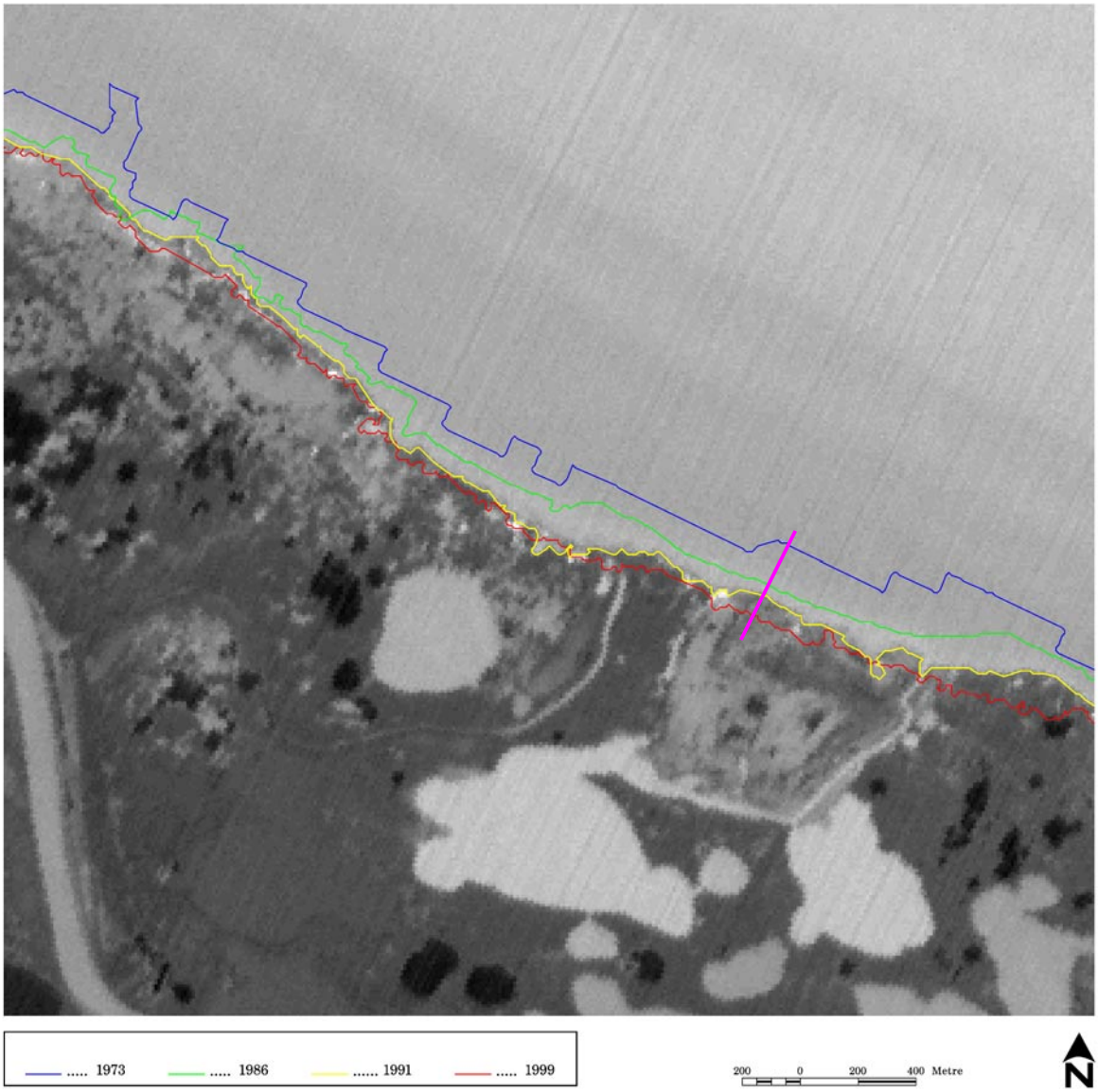

Figure 6.2 Derived coastlines shown on geocoded 1991 SPOT image for a rapidly eroding area (location 2 in figure 6.3), with pink line indicating transect used for figure 6.4.

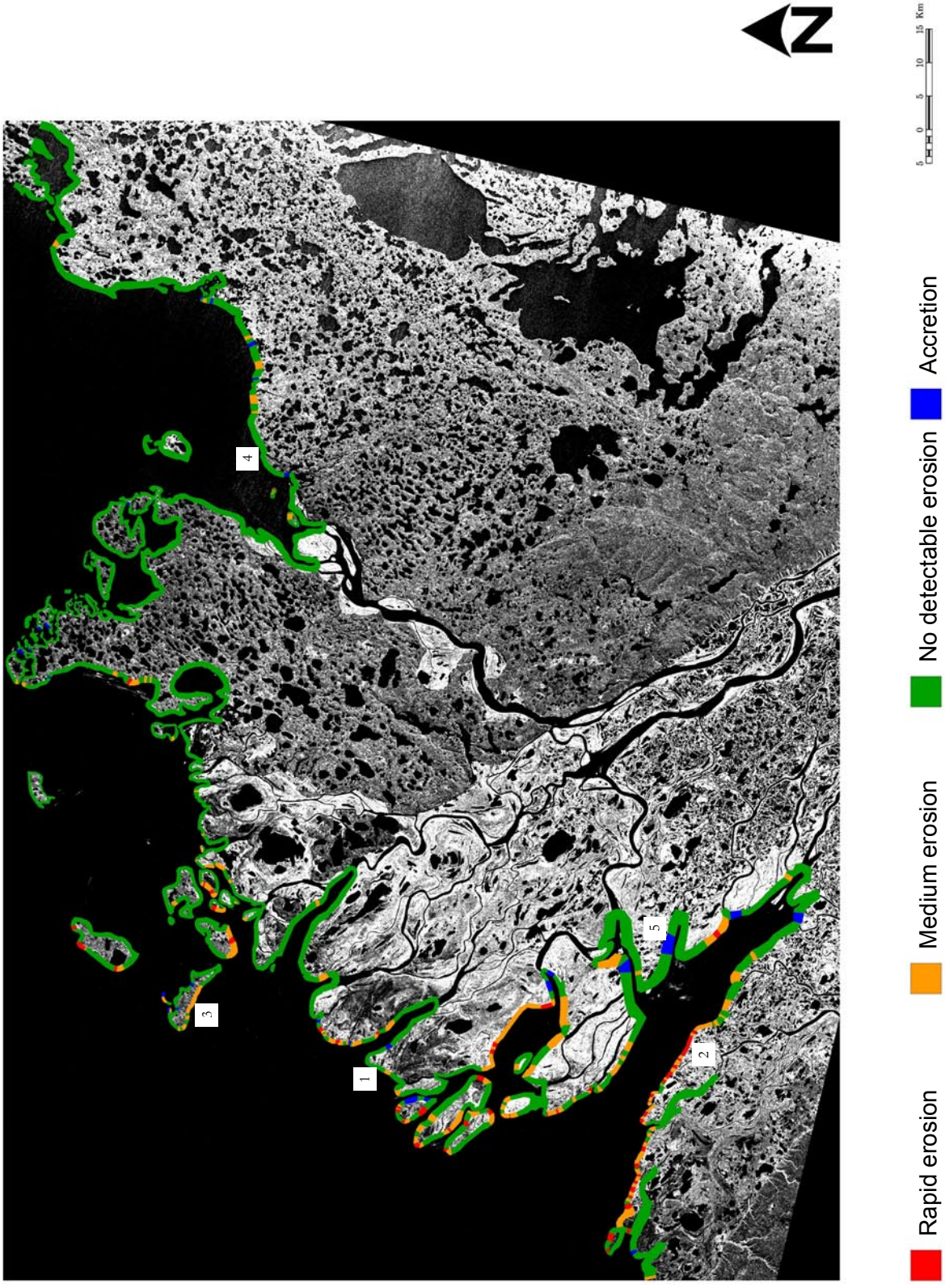

Figure 6.3 Erosion classes derived from coastlines on processed RADARSAT W2 image with numbers referring to the locations of figures 6.1, 6.2, and 6.4.

Apart from accelerating thaw settling on the bluffs, the inflow of warm water also accelerates the melting of sea ice during spring. As a consequence, larger ice-free fetches exist that increase the storm surge. This increased storm surge will accelerate coastal erosion (Solomon and Covill, 1995). What should be stressed is that storm winds mainly originate from the northwest. Many of the erosional areas are oriented towards this direction. Taking into account the northwest storm direction, it may be well possible that warm water flowing into the sea north of Shallow Bay (e.g. near Ellice Island) effectively contributes in creating relatively large ice-free fetches for the south shore of the Shallow Bay early in the open water season (and thus increase erosion). A complementary explanation for the high erosion rates may be the constriction of the water body (looking again from the northwest) going from the sea towards the bay. This constriction may have an additional raising effect on the storm surges as it acts like a funnel.

It is likely that erosion found outside the delta is also controlled by temperature related processes. For an accurate analysis of the factors causing coastal erosion, figure 6.3 should be compared with additional spatial data, concerning coastal types, permafrost characteristics, cliff height, and the composition of cliff and beach material. However, this is outside the scope of this project.

It should be stressed again that this study has been dealing with linear erosion. Although linear erosion rates may be high in the active delta, it is well possible that volumetric erosion rates are higher elsewhere, even where erosion could not be identified. As to present, no satellite remote sensing studies have been executed that investigate volumetric erosion of coastlines. It would imply that either a way needs to be found to estimate cliff height, or accurate Digital Elevation Models (DEM's) should be created and subtracted to identify volume loss. The estimation of cliff height could be done using additional databases or detailed contour maps. DEM's could be constructed by using for example stereoscopy or radar interferometry (Toutin and Gray, 2000). Future developments, as for instance the planned RADARSAT-2/3 topographic mapping mission (Reeves, 2000), will allow the creation of high accuracy DEM's, which will facilitate volumetric coastal erosion studies.

Figure 6.4 shows the linear change in coastline at four locations (see figure 6.3) corresponding to the identified erosion classes. Error bars reflect type 1 errors, which are estimated to be equal to the respective image resolutions. At location 3 the error bars overlap, yet the consistent trend of coastline retreat strongly suggests an erosion pattern. However, a clearer indication of erosion rates than shown in table 6.1 cannot be given for most locations, which can be illustrated by calculating the erosion rate and its error for location 2. Using the error bars to reflect the uncertainty in the estimate, the erosion rate ranges from 6 to 14 m yr^{-1}. Because of this uncertainty, it was chosen not to distinguish more erosion classes than presented in table 6.1.

The uncertainties in the positional accuracy of the extracted coastlines are considered too high to make conclusive assessments of possible temporal differences in rates of coastline change. Therefore, the results of the study can neither confirm nor refute the supposed acceleration in coastal retreat due to global warming (Solomon *et al.*, 1993). Given the rather slow pace of the climate change process, the time period covered by the available data (26 years) is also rather short. Future monitoring of coastal erosion will again benefit from the recent and forthcoming introduction of high-resolution satellites.

When a higher accuracy is attained, more precise coastal erosion rates can be calculated for different time spans at every location and subsequently compared. This will allow a proper assessment of the possible acceleration of erosion in the area. Nevertheless, this study does show that satellite remote sensing can be used effectively for coastal erosion studies. Considering the growing data availability and increasing resolution of present and future sensors, coastal erosion mapping can become an increasingly important application of remote sensing satellites.

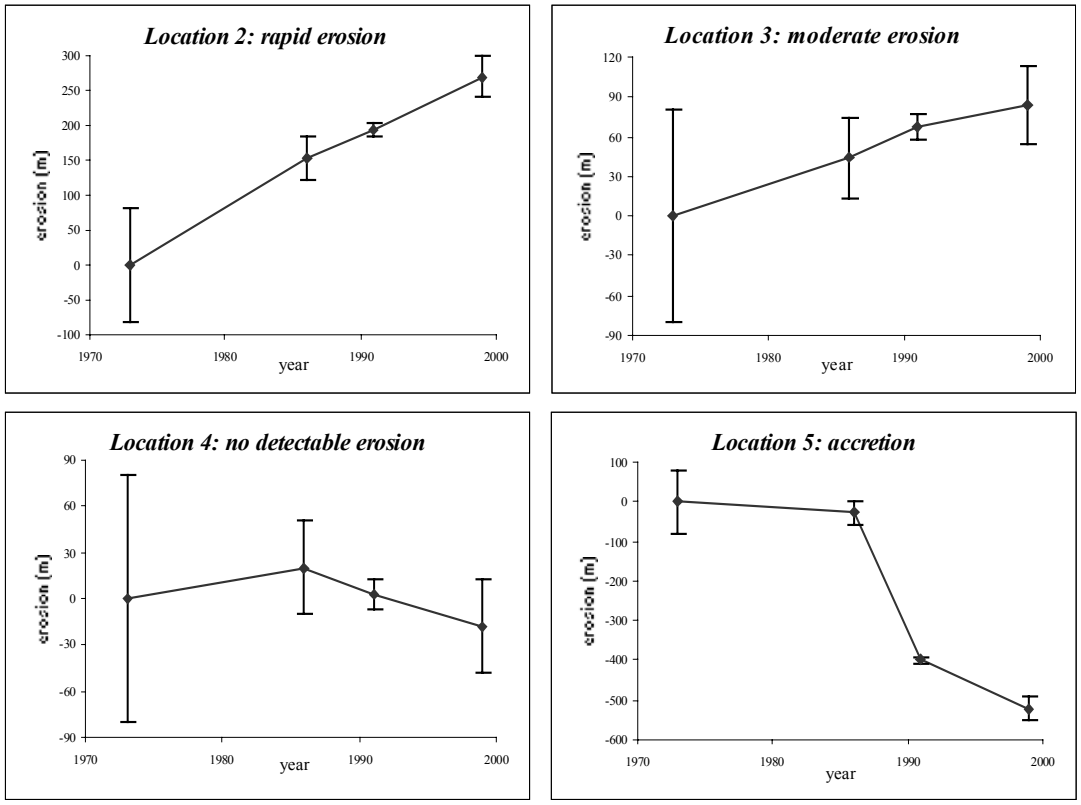

Figure 6.4 Graphs showing change in coastline at 4 spots in the area (see figure 6.3), as derived from the satellite images.

7. Conclusions and recommendations

The objectives of this study were (a) to develop a procedure for coastline extraction from a variety of satellite remote sensing data and (b) to map the coastline dynamics of the Canadian Beaufort Sea coast. Coastline extraction was achieved with the local region growing approach. This semi-automated method proved to function well for the varying image characteristics. More advanced algorithms are not expected to perform better than the applied approach, because of the complexity of the area and the imagery. The area has a highly irregular and at places poorly defined coastline. Moreover certain image regions show reduced land-water contrast due to a wind-roughened sea (radar) or the sediment load of the water (optical). Through comparison of the extracted coastlines, a map that reflects the coastline dynamics of the Canadian Beaufort Sea coast could be constructed. The study demonstrates that satellite remote sensing can effectively be used for coastal erosion analyses.

The coastal erosion map produced comprises four classes: rapid erosion (> 5 m yr^{-1}), moderate erosion (1-5 m yr^{-1}), no detectable erosion (-1 - 1 m yr^{-1}), and accretion (<-1 m yr^{-1}). More classes were not distinguished because of the possible inaccuracies in the position of the derived coastline vectors. The map shows more erosion for the active delta than for the coastal plains. Although this is confirmed in literature (Harper, 1990), it is recommended to compare the map with ground data or aerial photography studies to assess its accuracy. Additional ground reference data would contribute considerably to a detailed assessment of the erosion controlling factors in the area and as such support the modelling of the impact of climate changes. These data should comprise information on coastal types, permafrost characteristics, cliff height, and the composition of cliff and beach material. Some of these data are likely to be available in the Canadian Coastal Information System of the GSC Atlantic.

In years to come, the possibilities for the monitoring of coastal dynamics by means of satellite remote sensing are expected to improve. This is explained from (a) the increasing time span for which data will become available, (b) the expansion of the available image database as more satellites are being launched, and (c) the introduction of satellites with enhanced spatial resolutions. This will allow a more effective monitoring of coastal retreat rates, which assists in studying global warming effects.

Different sensors will image the same scene in different ways. Application of data from multiple sensor systems may therefore give rise to interpretation errors. Hence, it is recommended to use images acquired by one particular satellite or by satellites with similar specifications.

Recently, more and more earth observation satellites are becoming available. This raises the question what sensor type can be used best. The sensor choice depends among others on the required accuracy. The accuracy should at least be high enough to allow for detection of changes over the time span considered. This may imply an *a priori* estimation of expected coastal retreat rates. It is obvious that high spatial resolution imagery provides the highest sensitivity to coastline change, as the images contain a high level of detail. Especially when it is foreseen to monitor changes in retreat rates, or a detailed erosion map is required, it is recommended to use high-resolution images. Unfortunately, high spatial resolution is achieved at the expense of spatial coverage. Therefore, if the study area is large and only a general idea is required of the distribution of erosion, it is more economical to use data of a lower resolution.

Besides a decision on resolution requirements, it will also have to be decided whether to use optical or radar imagery. Radar has the capability to image through clouds, but backscatter is influenced by wind-roughened water, which diminishes the contrast between land and sea. Optical imagery is hindered by clouds and is influenced by sediment load in the water, which also deteriorates land-water contrast. The influence of sediment is less when larger wavelengths are used, like near IR, or

preferably mid IR. For example, Landsat TM band 7 shows a clear contrast between land and water. Hence, it is recommended to use either infrared bands of optical imagery or radar imagery for coastal erosion studies. In the optical case, images with acceptable cloud cover will have to be selected, whereas for the radar case, images taken during low wind conditions are preferred.

Coastal erosion studies typically require a considerable time series of images. This dictates the use of older satellite systems, and as such it hampers the exploitation of recent developments in satellite remote sensing technology. However, over time these new technologies will become increasingly useful and important.

To date, the Landsat TM satellite series has been in orbit the longest. Starting in 1982 with Landsat-4 up to present with Landsat-7, images have been acquired at 30 m resolution. Especially band 7 of this sensor is useful for coastline extraction. Landsat TM is a good option for providing an overview of erosion areas. The SPOT satellites provide imagery since 1986. Although the panchromatic mode is sensitive to sediment load, the near IR band of the multispectral mode (having 20 m resolution) are well suited for coastline extraction. SPOT-4, launched in 1998, has an additional mid IR band, which enhances the land-water contrast. Because of its higher spatial resolution, coastline extraction from SPOT can result in a higher accuracy compared to Landsat TM.

In the radar domain, two satellite systems presently enable coastal erosion studies. ERS-1 and 2 were launched in 1991 and 1995 respectively. The ERS-2 satellite is still in orbit, and therefore ERS images provide continuous coverage from 1991 onwards. ERS has a spatial resolution of about 30 m. Its low incident angle and the VV-polarisation result in a high backscatter from the sea under many circumstances. This can cause low contrast between land and sea. VV-polarisation is known to have a higher backscatter from water than HH-polarisation, used by RADARSAT-1. RADARSAT-1 was launched in 1995 and thus cannot cover more than 5 years. It can collect data under varying incident angles and at different resolutions (see figure 4.2). It is recommended to select high incident angles to optimise land-sea contrast. The selected resolution has implications on the area that can be covered with one image. The highest resolution is about 8.4 m for the fine beam modes, which can be used for detailed studies. For studies aiming at an overview of erosion areas, it is recommended not to use a coarser resolution than the wide beam mode (about 30 m). The use of RADARSAT is recommended over ERS, as land-sea contrast is usually clearer with high incident angles and HH-polarisation.

Recent technological developments will greatly influence the level of detail that can be studied with satellite remote sensing. The mentioned systems will improve and expand their possibilities and new very high-resolution systems are being launched. The follow-up of ERS (ENVISAT-1) will have multiple incident angles and the possibility to image in HV-polarisation. HV is known to show a better land-water contrast than HH or VV. RADARSAT-2 (planned for 2003) will also be able to image in HV-polarisation. Moreover this satellite will have an ultra fine 3 m resolution mode. SPOT-5, to be launched in 2001 will have a 2.5 and 5 m resolution panchromatic sensor, and a 10 m resolution multispectral scanner, including a near IR band. In 1999, IKONOS was launched, having a 1 m resolution panchromatic mode, and a 4 m resolution multispectral scanner (including near IR). Similar satellites will be launched in 2001 (QuickBird-2, OrbView-3/4). The EROS A1/2 are about to be launched and have a resolution of 1.8 m (panchromatic), whereas the EROS B-satellites, planned for launch between 2002-2004, will have a panchromatic mode with 0.82 m resolution. These new very high-resolution satellites will accommodate highly detailed coastal erosion studies.

The above shows that the possibilities to use satellite remote sensing for coastal erosion studies are increasing. For these studies to be successful it is recommended to first determine the coastal detail required based upon the study objectives and anticipated erosion rates. The level of detail depends on the data applied. Data selection is therefore the key factor for an accurate coastal erosion analysis.

References

Barbosa, M.P., Singhroy, V., and R. Saint-Jean, 1999. Mapping coastal erosion in southern Paraíba, Brazil from Radarsat-1. *Canadian Journal of Remote Sensing* 25-3, pp. 323-328.

Bijaoui J., and F. Cauneau, 1994. Separation of sea and land in SAR images using texture classification. *In:* Proceedings of IEEE Oceans 94 Conference, Brest, France, Vol. 1, pp. 522-526.

Bird, E.C.F., 1985. Coastline changes: a global review. J.Wiley & Sons, New York.

Blodget, H.W., Taylor, P.T., and J.H. Roark, 1991. Shoreline changes along the Rosetta-Nile promontory: monitoring with satellite observations. *Marine Geology* 99, pp. 67-77.

Burgess, M., Judge, A., Taylor, A., and V. Allen, 1982. Ground temperature studies of permafrost growth at a drained lake site, Mackenzie Delta. *In:* French, H.M. (ed.) Proceedings of 4th Canadian Permafrost Conference (Calgary), pp. 3-11.

Canny, J.F., 1986. A computational approach to edge detection. *IEEE Transactions on Pattern Analysis and Machine Intelligence* 8, pp. 679-698.

Chellappa, R., and A. Jain, 1993. Markov Random Fields: theory and application. Academic Press, New York.

Chen, A.J., Chen, C.F., and K.S. Chen, 1995. Investigation of shoreline change and migration along Wai-San-Ding-Zou barrier island, central western Taiwan. Proceedings IGARSS '95, Vol. 3, pp. 2097-2099.

Chen, L.C., and J.Y. Rau, 1998. Detection of shoreline changes for tideland areas using multi-temporal satellite images. *International Journal of Remote Sensing* 19-17, pp. 3383-3397.

Ching, W.S., 1994. A novel change detection algorithm using adaptive threshold. *Image and Vision Computing* 12, pp. 459-463

Dallimore, S. R., Wolfe, S., and S.M. Solomon, 1996. Influence of ground ice and permafrost on coastal evolution, Richards Island, Beaufort Sea Coast, NWT. *Canadian Journal of Earth Sciences* 33, pp. 664-675.

Davies, K.F., 1975. Mackenzie River input to Beaufort Sea. Fish. Oceans Canada, Sidney, B.C., Beaufort Sea Project, Technical Report 15.

De Abreu, R., Dallimore, S., Solomon, S., Edwardson, K., and C. Bjerkelund, *in preparation*. Monitoring spring ice break-up in the outer Mackenzie Delta with RADARSAT-1.

Descombes, X., Moctezuma, M., Maître, H., and J.P. Rudant, 1996. Coastline detection by a Markovian segmentation on SAR images. *Signal Processing* 55, pp. 123-132.

Dolan, R., Hayden, B., and J. Heywood, 1978. A new photogrammetric method for determining shoreline erosion. *Coastal Engineering* 2, pp. 21-39.

El Raey, M., Sharaf El Din, S.H., Khafagy, A.A., and A.I Abo Zed, 1999. Remote sensing of beach erosion/accretion patterns along Damietta-Port Said shoreline, Egypt. *International Journal of Remote Sensing* 20, pp. 1087-1106.

Energy, Mines and Resources Canada, 1988. Mackenzie Delta, District of Mackenzie, Northwest Territories. Topographic map, scale 1:250000.

Energy, Mines and Resources Canada, 1989a. Blow River, Yukon Territory, Northwest Territories. Topographic map, scale 1:250000.

Energy, Mines and Resources Canada, 1989b. Herschel Island, Yukon Territory, Northwest Territories. Topographic map, scale 1:250000.

Frihy, O.E., Dewidar, K.M., Nasr, S.M., and M. El Raey, 1998. Change detection of the northeastern Nile Delta of Egypt: shoreline changes, spit evolution, margin changes of Manzala lagoon and its islands. *International Journal of Remote Sensing* 19, pp. 1901-1912.

Frihy, O.E., Nasr, S.M., El Hattab, M.M., and M. El Raey, 1994. Remote sensing of beach erosion along Rosetta promontory northeastern Nile Delta, Egypt. *International Journal of Remote Sensing* 15, pp. 1649-1660.

Grotefendt, K., Logemann, K., Quadfasel, D., and S, Ronski, 1998. Is the Arctic Ocean warming? *Journal of Geophysical Research* 103-C12, pp. 27679-27687.

Hanson, H., 1993. Coastal erosion: an escalating environmental threat. *Ambio* 22-4, pp. 188-195.
Harper, J.R, 1990. Morphology of the Canadian Beaufort Sea Coast. *Marine Geology* 91, pp. 75-91.
Harper, J.R., Henry, R.F., and G.G. Stewart, 1988. Maximum storm surges elevations in the Tuktoyaktuk region of the Canadian Beaufort Sea. *Arctic* 41, pp. 48-52.
Harper, J.R., Reimer, P.D., and A.D. Collins, 1985. Canadian Beaufort Sea physical shore-zone analysis. Geological Survey of Canada. Open-file report 1689.
Hayes, M.O., 1979. Barrier island morphology as a function of tidal and wave regime. *In:* Leatherman, S.E. (ed.) Barrier Islands: from the Gulf of St. Lawrence to the Gulf of Mexico. Academic Press, New York, pp. 1-27.
Henderson, F.M., and A.J. Lewis (eds.), 1998. Principles and applications of imaging radar; Manual of Remote Sensing (3rd ed.) Vol. 2. J.Wiley & Sons, New York.
Héquette, A., and P.W. Barnes, 1990. Coastal retreat and shoreface profile variations in the Canadian Beaufort Sea. *Marine Geology* 91, pp. 113-132.
Hill, P.R., Barnes, P.W., Héquette, A., and M-H Ruz, 1994. Arctic coastal plain shorelines. *In*: Carter, R.W.G., and C.D. Woodroffe (eds.). Coastal Evolution: Late Quaternary shoreline morphodynamics. Cambridge University Press, Cambridge, England.
Hill, P.R., Héquette, A., and M-H. Ruz, 1993. Holocene sea-level history of the Canadian Beaufort shelf. *Canadian Journal of Earth Sciences* 30, pp. 103-108.
Hill, P.R., and S.M. Solomon, 1999. Geomorphologic and sedimentary evolution of a transgressive thermokarst coast, Mackenzie Delta Region, Canadian Beaufort Sea. *Journal of Coastal Research* 15-4, pp. 1011-1029.
Hunter, J.A., 1988. Permafrost aggradation and degradation on Arctic coasts of North America. Proceedings of 5th International Permafrost Conference, Trondheim, Norway, Vol. 3, pp. 27-34.
Johannessen, O.M., Miles, M., and E. Bjørgo, 1995. The Arctic's shrinking sea ice. *Nature* 376, pp. 126-127.
Kass, M., Witkin, A., and D. Terzopoulos, 1987. Snakes: active contour models. *International Journal of Computer Vision* 1, pp. 321-331.
Kobayashi, N., and D. Atkan, 1986. Thermoerosion of frozen sediment under wave action. *Journal of Waterway, Port, Coastal and Ocean Engineering* 112, pp. 140-158.
Kobayashi, N., Vidrine, J.C., Nairn, R.B., and S.M. Solomon, 1999. Erosion of frozen cliffs due to storm surge on Beaufort Sea coast. *Journal of Coastal Research* 15-2, pp. 332-344.
Kurfurst, P.J., and S.R. Dallimore, 1991. Engineering geology of nearshore areas off Richards Island, N.W.T.: a comparison of stable and actively eroding coastlines. *Canadian Geotechnical Journal* 28, pp. 179-188.
Lee, J.S., and I. Jurkevich, 1990. Coastline detection and tracing in SAR images. *IEEE Transactions on Geoscience and Remote Sensing* 28, pp. 662-668.
Le Moigne, J., and J.C. Tilton, 1995. Refining image segmentation by integration of edge and region data. *IEEE Transactions on Geoscience and Remote Sensing* 33, pp. 605-615.
Lie, W.N., 1995. Automatic target segmentation by locally adaptive image thresholding. *IEEE Transactions on Image Processing* 4, pp. 1036-1041.
Lillesand, T.M., and R.W. Kiefer, 1994. Remote sensing and image interpretation (3rd ed.). J.Wiley & Sons, New York.
Lira, J., and L. Frulla, 1998. An automated region growing algorithm for segmentation of texture regions in SAR images. *International Journal of Remote Sensing* 19, pp. 3595-3606.
Lopes, A., Nezry, E., Touzi, R., and H. Laur, 1993. Structure detection and statistical adaptive speckle filtering in SAR images. *International Journal of Remote Sensing* 14, pp. 1735-1758.
Lopes, A., Touzi, R., and E. Nezry, 1990. Adaptive speckle filters and scene heterogeneity. *IEEE Transactions on geoscience and remote sensing* 28, pp.992-1000.
Mackay, J.R., 1962. Pingos of the Pleistocene Mackenzie River delta area. *Geographical Bulletin* 18, pp. 21-63

Mackay, J.R., 1963. The Mackenzie Delta Area, N.W.T. Geographical Branch, Mines and Technical Surveys, Ottawa, Memoir 8, 202p.

Mackay, J.R., 1971. The origin of massive icy beds in permafrost, western Arctic, Canada. *Canadian Journal of Earth Sciences* 8, pp. 397-422.

Mackay, J.R., 1986. Fifty years (1935 to 1985) of coastal retreat west of Tuktoyaktuk, District of Mackenzie. *In:* Current Research, Part A, Geological Survey of Canada, Paper 86-1A, pp. 727-735

Majumbar, T.J., and B.B. Bhattacharya, 1991. Extraction of shoreline and drainage patterns from aerial MSS thermal IR data over Cambay Basin, India: an attempt to automatize the threshold selection. *Pattern Recognition* 24-2, pp. 157-164.

Mallat, S., and W.L. Hwang, 1992. Singularity detection and processing with wavelets. *IEEE Transactions on Information Theory* 38, pp. 617-643.

Mallat, S., and S. Zhong, 1992. Characterization of signals from multiscale edges. *IEEE Transactions on Pattern Analysis and Machine Intelligence* 14, pp. 710-732.

Mason, D.C., and I.J. Davenport, 1996. Accurate and efficient determination of the shoreline in ERS-1 images. *IEEE Transactions on Geoscience and Remote Sensing* 34-5, pp. 1243-1253.

Natural Resources Canada, 1996. Aklavik, District of Mackenzie, Northwest Territories. Topographic map, scale 1:250000.

Niedermeier, A., Romaneessen, E., and S. Lehner, 2000. Detection of coastlines in SAR images using wavelet methods. *IEEE Transactions on Geoscience and Remote Sensing* 38, pp. 2270-2281.

Oliver, C., and S. Quegan, 1998. Understanding synthetic aperture radar images. Artech House, Norwood, MA.

Pal, N.R., and S.K. Pal, 1993. A review on image segmentation techniques. *Pattern Recognition* 26, pp. 1277-1294.

Pilkey, O.H., 1991. Coastal erosion. *Episodes* 14-1, pp. 46-51.

Pinchin, B.M., Nairn., B., and K.L. Philpott, 1985. Beaufort Sea coastal sediment study: numerical estimation of sediment transport and nearshore profile adjustments at coastal sites in the Canadian Beaufort Sea. Open File Report 1259, Geological Survey of Canada.

Pirazolli, P.A., 1985. Sea-level change. *Nature and Resources, Vol. XXI.* Unesco, Paris.

Pollard, W.H., and Dallimore, S.R., 1983. Petrographic characteristics of massive ground ice, Yukon Coastal Plain, Canada. *In:* Proceedings of the 5th International Conference on Permafrost, Trondheim, Norway, pp. 224-229.

Pollard, W.H., and H.M. French, 1980. A first approximation of the volume of ground ice, Richards Island, Pleistocene Mackenzie delta, Northwest Territories, Canada. *Canadian Geotechnical Journal* 17, pp. 509-516.

Pratt, W.K., 1978. Digital image processing. J.Wiley & Sons, New York.

Quadfasel, D., Sy, A., Wells, D., and A. Tunik, 1991. Warming in the Arctic. *Nature* 350, pp. 385.

Rampton, V.N., 1982. Quaternary geology of the Yukon Coastal Plain. Geological Survey of Canada, Bulletin 317.

Rampton, V.N., 1988. Quaternary geology of the Tuktoyaktuk Coastlands, Northwest Territories. Geological Survey of Canada, Memoir 423.

Raney, R.K., 1998. Radar fundamentals: technical perspective. *In:* Henderson, F.M., and A.J. Lewis (eds.). Principles and applications of imaging radar; Manual of Remote Sensing (3rd ed.) Vol. 2. J.Wiley & Sons, New York.

Reeves, L.A., 2000. The RADARSAT-2/3 topographic mapping mission. *In:* Proceedings of the 11th Conference on Aeronautics ASTRO 2000, Ottawa, Ontario, Canada, pp. 375-378.

Romaneessen, E., Lehner, S., Niedermeier, A., and J. Horstmann, 2000. Morphodynamic in the Elbe estuary as seen by ERS synthetic aperture radar. *In:* Proceedings of the 6th International Conference on Remote Sensing for Marine and Coastal Environment, Charleston, South Carolina, Vol. 1, pp. 296-302.

Rumelhart, D.E., and J.L. McClelland, 1986. Parallel distributed processing. MIT Press, Cambridge, Massachusetts.

Ruz, M-H., Héquette, A., and P.R. Hill, 1992. A model of coastal evolution in a transgressed thermokarst topography, Canadian Beaufort Sea. *Marine Geology* 106, pg. 251-278.

Ryan, T.W., Sementelli, P.J., Yuen, P., and B.R. Hunt, 1991. Extraction of shoreline features by neural nets and image processing. *Photogrammetric engineering and Remote Sensing* 57-7, pp. 947-955.

Schwäbisch, M., Lehner, S., and N. Winkel, 1997. Coastline extraction using ERS SAR interferometry. Third ERS symposium, Florence, 17-20 March 1997. URL: http://earth.esa.int/florence/papers/program-details/data/schwaebisc/

Shaw, J., Taylor, R.D., Forbes, D.L., Ruz, M-H., and S. Solomon, 1994. Sensitivity of the Canadian coast to sea-level change. Open File Report 2825, Geological Survey of Canada.

Shi, Z., and K.B. Fung, 1994. A comparison of digital speckle filters. Proceedings IGARSS '94, Vol. 4, pp. 2129-2133.

Shoshany, M., and A. Degani, 1992. Shoreline detection by digital image processing of aerial photography. *Journal of Coastal Research* 8, pp. 29-34.

Singhroy, V., 1996. Interpretation of SAR images for coastal zone mapping in Guyana. *Canadian Journal of Remote Sensing* 22-3, pp. 317-328.

Solomon, S.M., and R. Covill, 1995. Impacts of the September 1993 storm on the Beaufort Sea. *In:* Proceedings of the 1995 Canadian Coastal Conference, Vol.2, pg. 779-795.

Solomon, S.M., Forbes, D.L., and B. Keirstead, 1993. Coastal impacts of climate change: Beaufort Sea erosion study. Open-File Report 2890, Geological Survey of Canada.

Stafford, D.B., and J. Langfelder, 1971. Air photo survey of coastal erosion. *Photogrammetric Engineering* 37, pp. 565-575.

Taxt, T., Flynn, P.J., and A.K. Jain, 1989. Segmentation of document images. *IEEE Transactions on Pattern Analysis and Machine Intelligence* 11, pp. 1322-1329.

Tou, J.T., and R.C. Gonzalez, 1979. Pattern recognition principles. Addison-Wesley Publishing, Reading, Massachusetts.

Toutin, T., and L. Gray, 2000. State-of-the-art of elevation extraction from satellite SAR data. *ISPRS Journal of Photogrammetry and Remote Sensing* 55, pp. 13-33.

Touzi, R., Lopes, A., and P. Bousquet, 1988. A statistical and geometrical edge detector for SAR images. *IEEE Transactions on geoscience and remote sensing* 26, pp. 764-773.

Walsh, J.E., 1991. The Arctic as a bellwether. *Nature* 352, pp. 19-20.

White, K., and H.M. El Asmar, 1999. Monitoring changing position of coastlines using Thematic Mapper imagery, and example from the Nile Delta. *Geomorphology* 29, pp. 93-105.

Zhang, D., Van Gool, L., and A. Oosterlinck, 1994. Coastline detection from SAR images. Proceedings IGARSS '94, Vol. 4, pp. 2134-2136.

Zhong, S., 1990. Edge representation from wavelet transform maxima. Ph.D. thesis, Department of Computer Science, New York University.

Zucker, S.W., 1976. Region growing: childhood and adolescence. *Computer Graphics and Image Processing* 5, pp. 382-399.